**Title: The temporal pattern of Intracortical Microstimulation pulses elicits distinct temporal and spatial recruitment of cortical neuropil and neurons.**

**Authors:** James R. Eles[1,*], Kevin C. Stieger[1-2,*], Takashi D.Y. Kozai[1-5#]

1. Department of Bioengineering, University of Pittsburgh, Pittsburgh, PA
2. Center for the Neural Basis of Cognition, University of Pittsburgh, Carnegie Mellon University, Pittsburgh, PA
3. Center for Neuroscience, University of Pittsburgh, Pittsburgh, PA
4. McGowan Institute for Regenerative Medicine, University of Pittsburgh, Pittsburgh, PA
5. NeuroTech Center, University of Pittsburgh Brain Institute, Pittsburgh, PA

* Equal Contribution
# Corresponding author: tdk18@pitt.edu

**Keywords:** neuromodulation, calcium imaging, brain stimulation, brain-computer interface, duty cycle, iGluSnFr, biomimetic

## 1. Abstract

Objective:
The spacing or distribution of stimulation pulses of therapeutic neurostimulation waveforms—referred to here as the Temporal Pattern (TP)—has emerged as an important parameter for tuning the response to deep-brain stimulation and intracortical microstimulation (ICMS). While it has long been assumed that modulating the TP of ICMS may be effective by altering the rate coding of the neural response, it is unclear how it alters the neural response at the neural network level. The present study is designed to elucidate the neural response to TP at the network level.

Approach:
We use *in vivo* two-photon imaging of ICMS in mice expressing the calcium sensor *Thy1*-GCaMP or the glutamate sensor *hSyn*-iGluSnFr to examine the layer II/III neural response to stimulations with different TPs. We study the neuronal calcium and glutamate response to two TPs with the same average frequency (10Hz) and same total charge injection, but varying degrees of bursting, and one pattern with an average frequency of 100Hz and 10X the charge injection as the other patterns.

Main Results:
Stimulation trains with the same average frequency (10 Hz) and same total charge injection but distinct temporal patterns recruits distinct sets of neurons. A majority (60% of 309 cells) prefer one temporal pattern over the other. Despite their distinct spatial recruitment patterns, both cells exhibit similar ability to follow 30s trains of both TPs without failing, and they exhibit similar levels of glutamate release during stimulation. Both neuronal calcium and glutamate release train to the bursting TP pattern (~21-fold increase in relative power at the frequency of bursting. Bursting also results in a statistically significant elevation in the correlation between somatic calcium activity and neuropil activity, which we explore as a metric for inhibitory-excitatory tone. Interestingly, soma-neuropil correlation during the bursting pattern is a statistically significant predictor of cell preference for TP, which exposes a key link between inhibitory-excitatory tone. Finally, using mesoscale imaging, we show that both TPs result in distal inhibition during stimulation, which reveals complex spatial and temporal interactions between temporal pattern and inhibitory-excitatory tone in ICMS.

Significance:
Our results may ultimately suggest that TP is a valuable parameter space to modulate inhibitory-excitatory tone as well as distinct network activity in ICMS. This presents a broader mechanism of action than rate coding, as previously thought. By implicating these additional mechanisms, TP may have broader utility in the clinic and should be pursued to expand the efficacy of ICMS therapies.

## 2. Introduction

Electrical stimulation has been widely used as a tool to study neuronal circuits [1], treat neurological disorders [2, 3], and produce artificial perception in brain machine interfaces [4-6]. Stimulation of thalamocortical circuits

(deep brain stimulation) can relieve symptoms of Parkinson's disease [2], auditory nerve stimulation can restore the ability to hear [7], and intracortical microstimulation (ICMS) can produce tactile[4, 8-10], proprioceptive [11], or visual perceptions [12-15] depending on the cortical location. Although these technologies have shown success in the clinic, there is a critical need to define the most effective stimulation parameters for a given outcome.

Varying stimulation parameters such as amplitude and frequency aim to modulate the population of neurons activated, as well as their firing rates and can affect the perception of the artificial sensation [16]. For example, non-human primates were able to discriminate between different uniform frequencies of intracortical microstimulation from electrodes implanted into the primary somatosensory cortex [9], but the effect of frequency on the quality of perception can be variable[17]. Additionally, stimulation frequency, amplitude, and train duration have all been suggested to modulate the perceived magnitude of the sensation [4, 5, 13, 16, 18]. However, although ICMS can reliably produce localized percepts [4-6, 14-16], stimulus amplitude has been suggested to have a nonlinear effect on the size of the receptive field [4, 13]. While stimulation amplitude and frequency can produce naturalistic sensations, sensory information is not always encoded in average firing rates [19-21]. Therefore, temporal patterning of electrical stimulation has emerged as a promising approach to encode more complex information [22].

The spacing or distribution of pulses over a stimulation train—referred here as the temporal pattern (TP) of electrical stimulation—has been suggested to have greater therapeutic potential in deep brain stimulation and may be able to produce more complex artificial perceptions [20, 22, 23]. Non-human primates are able to distinguish uniform stimulation frequency from temporally patterned stimulation of the somatosensory cortex suggesting that the pattern of stimulation modulates perceptual outcomes [5, 10, 24]. Additionally, temporal patterned stimulation of the visual cortex can prevent phosphene perception cessation observed with constant frequency stimulation [13]. Although temporally patterned stimulation can modulate perceptual quality and neuronal adaptation, there is a critical need to better understand how electrical stimulation can drive excitatory and inhibitory network activity.

Electrical stimulation results in a brief period of neuronal excitation followed by a downstream increase in inhibitory oscillations [25-34]. The strength and degree of inhibition can be modulated by stimulation trains with frequencies greater than 10 Hz [26]. Additionally, stimulation frequency can modulate the spatial recruitment and entrainment properties where neurons close to the electrode can follow trains ≤500 Hz, while more distal neurons have difficulty above 10 Hz [26, 28, 29, 31, 32]. In fact, this frequency-dependent fall off in activation can be clearly observed using calcium imaging to quantify the activity level during long (30s) stimulation trains [35-37]. It is possible that the strong excitatory drive at the onset of stimulation coupled with higher firing rates of GABAergic neurons produces a strong inhibitory build-up to cause this transient spatiotemporal activity and inactivation of neurons that may have been indirectly activated [35]. This would not be surprising considering that many cortical networks show inhibitory stabilization characteristics[38]. Therefore, careful consideration of cortical network tendency to balance excitation with inhibition could help design temporal patterned stimulation protocols that expand therapeutic potential of ICMS.

This is the first study to use *in vivo* two-photon imaging of mice expressing either the calcium sensor GCaMP6s or the glutamate sensor iGluSnFr in cortical neurons to compare the differential spatiotemporal dynamics of neuronal activation by stimulations of different TPs. Specifically, we examined the neural response to two TPs with the same average frequency (10 Hz) and same total charge injection, but one with bursts (10 Hz-Burst) and one with uniform pulses (10 Hz-Uniform). As a control, 100 Hz-Uniform stimulation (100 Hz) was used to drive the characteristic spatiotemporal fall off of neural activity (100Hz; patterns illustrated in Figure 1) and examine the spatiotemporal contribution of high frequency uniform ICMS on excitation and inhibition. Given that GCaMP6s activity increases with multiple action potential and decays on the order 100's of milliseconds, if all neurons can entrain at higher frequency extracellular electrical stimulation, then it is expected that 100Hz-Uniform would lead to the greatest level of GCaMP activity and 10 Hz-Uniform would lead to the least amount of activation. In contrast, if >10Hz stimulation leads to preferential inhibition (inhibitory neurons can entrain to higher frequency stimulation), 100Hz-Uniform and 10Hz-Burst would be expected to evoke the least amount of GCaMP6s activity. Long stimulation trains (30 s) provided sufficient time for the build-up of inhibitory network oscillations and to observe key spatiotemporal activity patterns of cortical neurons that provide evidence for differential drive of excitatory or inhibitory network activity.

Using similar stimulation waveforms to those employed clinically[4, 39], we found that select neuronal populations preferred (*i.e.* stronger response) different TPs with 60% of cells having increased calcium activity in either 10Hz-Burst or 10Hz-Uniform compared to the other. Importantly, this effect was spatially- and charge injection-independent suggesting the TPs were driving distinct network activity. While the temporal activity between 10 Hz-Uniform and 10 Hz-Burst was similar, cells were able to entrain to the bursting of 10Hz-Burst, showing a 21-fold increase in relative 1Hz power (the bursting frequency) compared to the 10 Hz-Uniform or 100Hz patterns in addition to increased glutamate activity near the electrode. Furthermore, we demonstrate that TP preference arises from increased correlation between neuronal somas and the neuropil at the same distance. Finally, using mesoscale imaging, we show that 10 Hz-Burst and 100 Hz stimulation result in substantial inhibition at distant locations during the stimulation train. Ultimately, this work demonstrating the spatiotemporal differences in neuronal, neuropil, and glutamate activity indicates that there are previously unconsidered mechanisms for TP to be effective in ICMS. The TPs also shed light on the mechanisms that govern Onset and Steady State activation observed in constant high frequency stimulation (eg. 100 Hz). By exploring the temporal pattern parameter space, the therapeutic use of ICMS could be expanded to improve treatment in a growing patient population.

## Methods

## 3. Materials and Methods

### *3.1. Animals and virus injection*

Mature (>8 weeks and >25g) male mice were used for this study. Animals had free access to food and water and were housed in 12 h light/dark cycles. Transgenic mice expressing the calcium sensor GCaMP6S controlled by the Thy-1 promoter were used for experiments tracking neuronal calcium (6 animals; C57BL/6J-Tg(Thy1-GCaMP6s)GP4.3Dkim/J; Jackson Laboratories, Bar Harbor, ME) [40]. C57BL/6J mice with viral expression of a glutamate sensor were used for experiments measuring glutamate release (5 animals; Jackson Laboratories). These mice received intracortical viral injections of the glutamate sensor iGluSnFr with neuronal expression controlled by the hSyn promoter 3-8 weeks prior to implantation. The vector, pAAV.hSyn.iGluSnFr.WPRE.SV40, was a gift from Loren Looger (Addgene viral prep # 98929-AAV1; http://n2t.net/addgene:98929 ; RRID:Addgene_98929) [41]. Virus was delivered following a unilateral craniotomy with ketamine/xylazine anesthesia (75 mg/kg to 7mg/kg, respectively). Virus was bolus injected into visual and somatosensory cortices under aseptic conditions as previously described [42]. Bolus injection was completed with a glass micropipette controlled by a pressure injector to a volume of <1µL per site. All craniotomies were hermetically sealed with a silicone elastomer (KwikSil, World Precision Instruments) and a coverglass. A metal frame was cemented to the skull to allow facile monitoring of iGluSnFr expression. For 72h following surgical intervention, subjects received daily injections of ketoprofen (5 mg/kg). All experimental protocols were approved by the University of Pittsburgh Division of Laboratory Animal Resources and Institutional Animal Care and Use Committee in accordance with the standards for humane animal care as set by the Animal Welfare Act and the National Institutes of Health Guide for the Care and Use of Laboratory Animals.

### *3.2. Electrodes and implantation*

Acute-style single-shank 16-channel Michigan style functional silicon probes with 703 $\mu m^2$ electrode sites were used for all experiments (A1x16-3mm-100-703; NeuroNexus, Ann Arbor, MI). All iridium sites were activated to iridium oxide by published protocols [43]. All sites were confirmed to have <500kOhm 1kHz impedance prior to experiment. The electrode implantation procedure followed our previously optimized acute-implantation strategy for simultaneous two-photon imaging [42, 44-52]. Animals received IP injections of ketamine/xylazine for anesthesia (75 mg/kg to 7 mg/kg, respectively) and were then head-fixed into a stereotaxic frame. Subjects were maintained with a heating pad, $O_2$ line, and subcutaneous lactated Ringer's solution injections for long experiments (>6h). Anesthesia was updated approximately every hour with 45 mg/kg ketamine. After subjects reached an anesthetic plane, their scalps were removed, and a stainless-steel bone screw was drilled into the skull over the motor cortex. This served as a counter electrode and ground for all electrical stimulation. Bilateral craniotomies (3-5$mm^2$) were created by high-speed drill over somatosensory and visual cortices. The dura mater was carefully removed with fine forceps. The electrode implantation site was selected to be a region with limited vascular coverage in somatosensory cortex to avoid bleeding [53]. Electrodes were implanted at a 30$^o$ angle with an oil-hydraulic Microdrive (MO-81, Narishige, Japan) at 200 µm/s to a depth of

250-300 μm to reach layer II/III of cortex. Throughout the procedure, the surface of the brain was kept hydrated with sterile saline.

*3.3. Stimulation Paradigms*

All stimulation was carried out with an IZ2 stimulator under control of an RZ5D processor (Tucker-Davis technologies, Alachua, FL). The ICMS waveform consisted of a 100 μs, 15 μA (1.5 nC/phase) cathodic phase, a 50 μs interphase period of 0 μA, and a 200 μs, 7.5 μA anodic phase. Stimulation trains were 30s with at least a 90s delay between stimulations [35, 44]. Stimulation varied by the temporal patterning (TP) of the ICMS train (illustrated in Figure 1B). Two patterns (10 Hz-Burst and 10 Hz-Uniform) had the same average frequency of 10 Hz and same overall charge injection, but that vary in the bursting pattern, and a third pattern had an average frequency of 100Hz and had 10X the amount of charge injection as 10 Hz-Burst and 10 Hz-Uniform. 10 Hz-Burst consisted of 100ms bursts of 100Hz stimulation every second (resulting in an average frequency of 10Hz), while 10 Hz-Uniform consisted of steady pulses at 10Hz. These patterns were selected because previous studies demonstrated that 10 Hz and 100 Hz stimulation lead to significantly distinct spatiotemporal patterns of activation [32]. In addition, 100 Hz is used as a standard frequency in human S1 ICMS [54]. Similarly, 30 s was chosen because electrical stimulation onset effects have been previously reported to last ~20 as discussed in [32]. For ground and counter electrodes, a stainless-steel bone screw was placed with contact to the motor cortex.

*3.4. Imaging*

Imaging was performed either with an MVX-10 epifluorescence microscope (Olympus, Tokyo, Japan) with a CCD camera (Retiga R1, QI Imaging), or a two-photon microscope (Bruker, Madison, WI) with an OPO laser (Insight DS+; Spectra Physics; Menlo Park, CA) tuned to 920 nm. Laser power was kept under 40mW to prevent tissue damage. The two-photon scan-head was equipped with a 16X 0.8 NA water immersion objective (Nikon Instruments; Melville, NY). All two-photon imaging was set in resonance mode that collects 512 by 512 pixels (407 x 407 $\mu m^2$) at 30 frames per second while MVX-10 images were collected at 20 frames per second.

*3.5. Image analysis and statistics*

3.5.1. Stimulation Session Inclusion

A total of 6 stimulation sessions with the 10 Hz-Burst, 10 Hz-Uniform, and 100Hz patterns were processed for both the GCaMP6 (4 total animals) and iGluSnFr (4 total animals) groups. For one animal in the GCaMP6 group and two animals in the iGluSnFr groups, stimulations from separate implantation sites or electrode sites were used as separate trials for the analysis. For each session, there was minimal axial tissue displacement, and the same cells or landmarks could be identified through stimulation amplitude time series.

3.5.2. GCaMP6 soma quantification

Cell outlines were manually performed in ImageJ (NIH) using a 2D projection of the standard deviation of fluorescence [35, 44]. The mean fluorescence activity of each cell was extracted over the imaging session and exported to MATLAB (Mathworks, Boston, MA) for further analysis. To account for changes in baseline fluorescence, all traces were transformed to $dF/F_0$ using a mean of the pre-stimulation fluorescence (a 10s window) as baseline. To remove artifacts, $dF/F_0$ traces were low-pass filtered with a finite impulse filter ($10^{th}$ order) with a 1Hz cutoff frequency. A cell was considered as “active” if its’ $dF/F_0$ crossed a threshold of the mean pre-stimulus intensity + 2 standard deviations for at least 1s during stimulation. All active cells that sustained calcium activity for at $\geq$ 0.5s during the last 2s of stimulation were labeled as “Steady State” cells, while all other active cells were labeled as “Onset” cells. Cells that never crossed the “active” threshold were discounted from the study. Cumulative $dF/F_0$ was calculated as the integral of $dF/F_0$ over the entirety of the stimulation period for each temporal pattern. The relative 1Hz frequency of each cell for each temporal pattern was calculated by Fast Fourier Transform computed in MATLAB. Each cell’s position relative to the stimulation site was determined by a distance transformation. Cells were sorted into 20 μm bins extending from the perimeter of the stimulation site. All comparisons between cells by distance and temporal pattern or Onset/Steady State categorization were modeled by a two-way ANOVA. Post-hoc pairwise comparisons were carried out accounting for multiple comparisons with Tukey’s post-hoc test and a significance level of $p < 0.05$.

To determine a cell’s preference for a certain temporal pattern, we compared the cumulative $dF/F_0$ of a cell’s response to the different temporal patterns. For a 10 Hz-Burst v. 10 Hz-Uniform comparison, if a cell’s

cumulative $dF/F_0$ for either 10 Hz-Burst or 10 Hz-Uniform was over 2X greater than its response for the other pattern, it was considered to have a preference. To determine if a cell preferred the 100 Hz pattern over either 10 Hz-Burst or 10 Hz-Uniform, we compared the cumulative $dF/F_0$ of the 100Hz pattern to the larger of the 10 Hz-Burst or 10 Hz-Uniform cumulative response. If the 100Hz pattern response was ≥2X to the 10 Hz-Burst or 10 Hz-Uniform response or vice versa, the cell was determined to have a preference. Cells that did not cross the 2X threshold were considered to have no preference.

3.5.3. GCaMP6 neuropil quantification

After cell somas were selected, they could be masked out of the image to isolate the neuropil. For two-photon analysis, $dF/F_0$ of neuropil was calculated 20 μm bins extending out from the perimeter of the stimulation site [35, 44, 55, 56]. For mesoscale microscope analysis, $dF/F_0$ was calculated in bins of 60 μm. Cumulative $dF/F_0$ was calculated as described in 3.5.2. Change in mean $dF/F_0$ from 0-2s to 28-30s was calculated by subtracting the mean $dF/F_0$ for those periods. The relative 1Hz frequency of each neuropil bin for each temporal pattern was calculated by Fast Fourier Transform computed in MATLAB. The Pearson's Coefficient of Correlation (*R*) was also determined between the time-course $dF/F_0$ of each cell soma and the time-course $dF/F_0$ of neuropil bin in which that soma resided as described in our previous work [35]. All statistical comparisons were conducted with two-way ANOVAs using Tukey's post-hoc pairwise tests to account for multiple comparisons.

3.5.4. iGluSnFr neuropil quantification

As we have previously reported, iGluSnFr expression in layer II/III was largely present in the neuropil, with few cell bodies showing expression [35]. Thus, $dF/F_0$ for iGluSnFr was quantified in 20 μm bins in a similar fashion to GCaMP neuropil. Cumulative $dF/F_0$ during stimulation was calculated as the integral $dF/F_0$ during the stimulation period. The relative 1Hz frequency of each bin for each temporal pattern was calculated by Fast Fourier Transform computed in MATLAB. All metrics were compared between distance bins and temporal pattern by two-way ANOVA with Tukey's post-hoc pairwise comparison tests to account for multiple comparisons.

## 4. Results

Temporal patterning (TP) of ICMS trains is an area of growing interest in neuromodulation, but the underlying mechanisms of how TP may modulate neural recruitment are unknown. Given that ICMS stimulation parameters are an infinite parameter space, it is important to understand the mechanisms that govern TP ICMS in order to intelligently engineer ICMS patterns for specific applications and conditions. In the present work, we use *in vivo* imaging of animals expressing the calcium sensor GCaMP (with high selectivity for pyramidal cells [57]) or the glutamate sensor iGluSnFr in cortical neurons to understand how TP may influence spatial and temporal recruitment properties of neurons.

4.1. Temporal patterning of ICMS elicits distinct spatial recruitment of neurons

To study the spatial and temporal neural response to temporal patterned ICMS, we used *in vivo* two-photon microscopy to measure cortical neuronal calcium activity in Layer II-III pyramidal cells of the somatosensory cortex (Figure 1). Temporal pattern was explored with two distinct stimulation trains with identical charge injection and an average frequency of 10 Hz: 10 Hz-Uniform, with 10 evenly spaced pulses every second, and 10Hz-Burst, with 10 pulses at 10ms intervals followed by 900ms of silence every second. These 1s periods were repeated 30 times for a 30 s ICMS train. A third pattern consisting of uniform 100Hz pulses (10X the charge injection of the other patterns) was examined as a positive control for a stimulation pattern that causes neuronal entrainment failure. All stimulation trains lasted 30 s to allow sufficient time to observe network activity and entrainment failure.

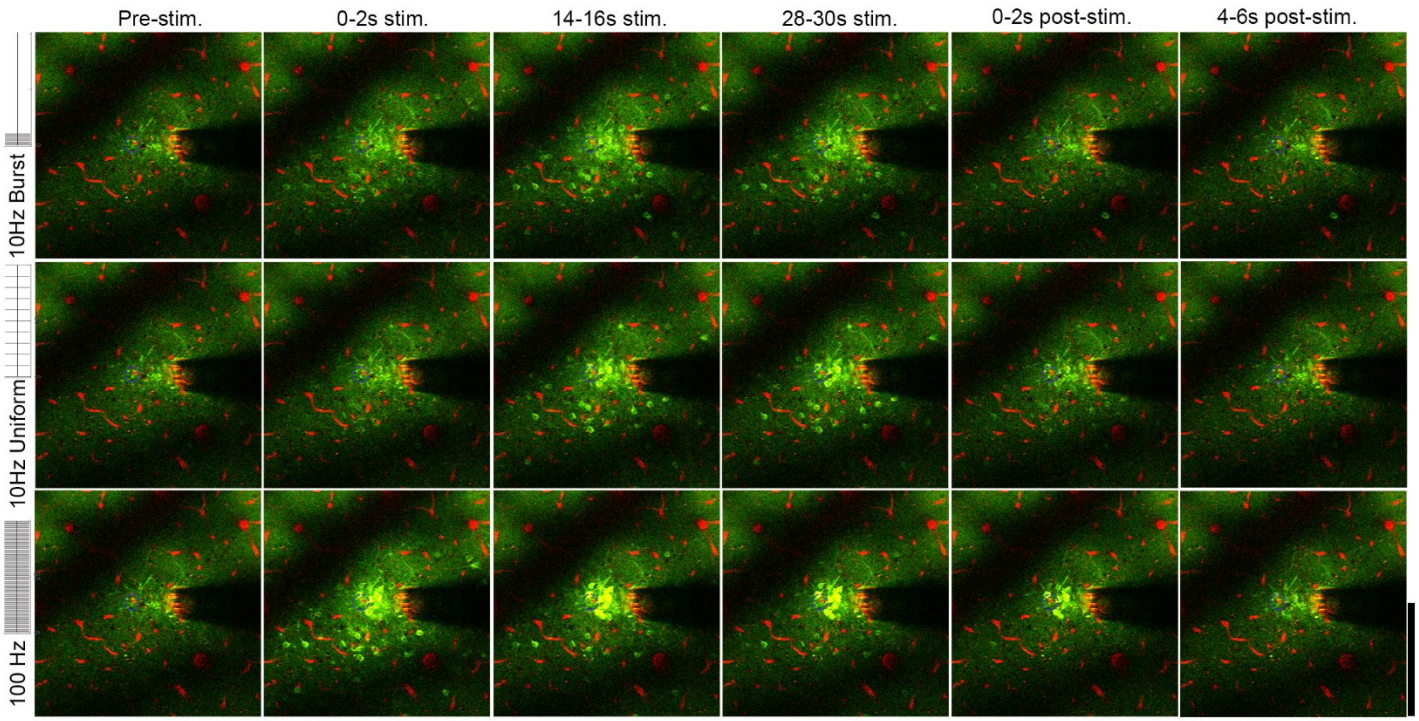


**Figure 1: Two-photon microscopy indicates reveals distinct spatial and temporal responses for neurons with 10Hz-Burst, 10 Hz-Uniform and 100Hz stimulation.** There is sustained neural activation both close and far from the electrode for 10Hz-Burst and 10 Hz-Uniform stimulation, while distant cells are only activated during 0-2s (onset period) for the 100 Hz pattern. Images are presented as averages over the indicated time periods. See supplemental Movies 1-3. The Thy-1 GCaMP is colored in green. Vasculature is labeled in red with sulforhodamine 101. The electrode site being stimulated is indicated by the blue dashed circle. Brightness and contrast are unmodified between images. Scale bar is 200 μm.

We hypothesized that temporal patterning would influence temporal coding of the neural response. Theoretical and experimental evidence has indicated that temporal coding in the cortex is controlled by a delicate balance of inhibitory and excitatory input [58]. Tuning of the inhibitory-excitatory balance in turn determines which cells are active in temporally coded activation [59-61]. In this vein, we observed that there was distinct spatial recruitment during 10 Hz-Burst and 10 Hz-Uniform stimulation (Figure 2A-B; Supplemental Movies 1-2). Many neurons showed a preferential response to either the Burst or Uniform pattern. To quantify the extent of this, we conservatively classified “preference” as a cell with cumulative calcium fluorescence that was 2X greater for one pattern than the other. Figure 2C illustrates examples of cells that have a preference for 10 Hz-Uniform and 10Hz-Burst. Cells that did not exceed this 2X difference were considered as having “no preference”. Interestingly, there was no trend for cell counts across distance from the electrode or across cell preferences (two-way ANOVA: $p > 0.05$; Figure 2D). This indicates that the distinct spatial recruitment between temporal patterns is not dictated by a simple distance relationship from the stimulation source, but rather something more complex. Finally, we quantified preference in 309 cells across 5 animals and 6 implantation sites to determine that a majority of cells (60%) preferred either the 10Hz-Burst pattern (31%) or the 10 Hz-Uniform pattern (29%) (Figure 2E).

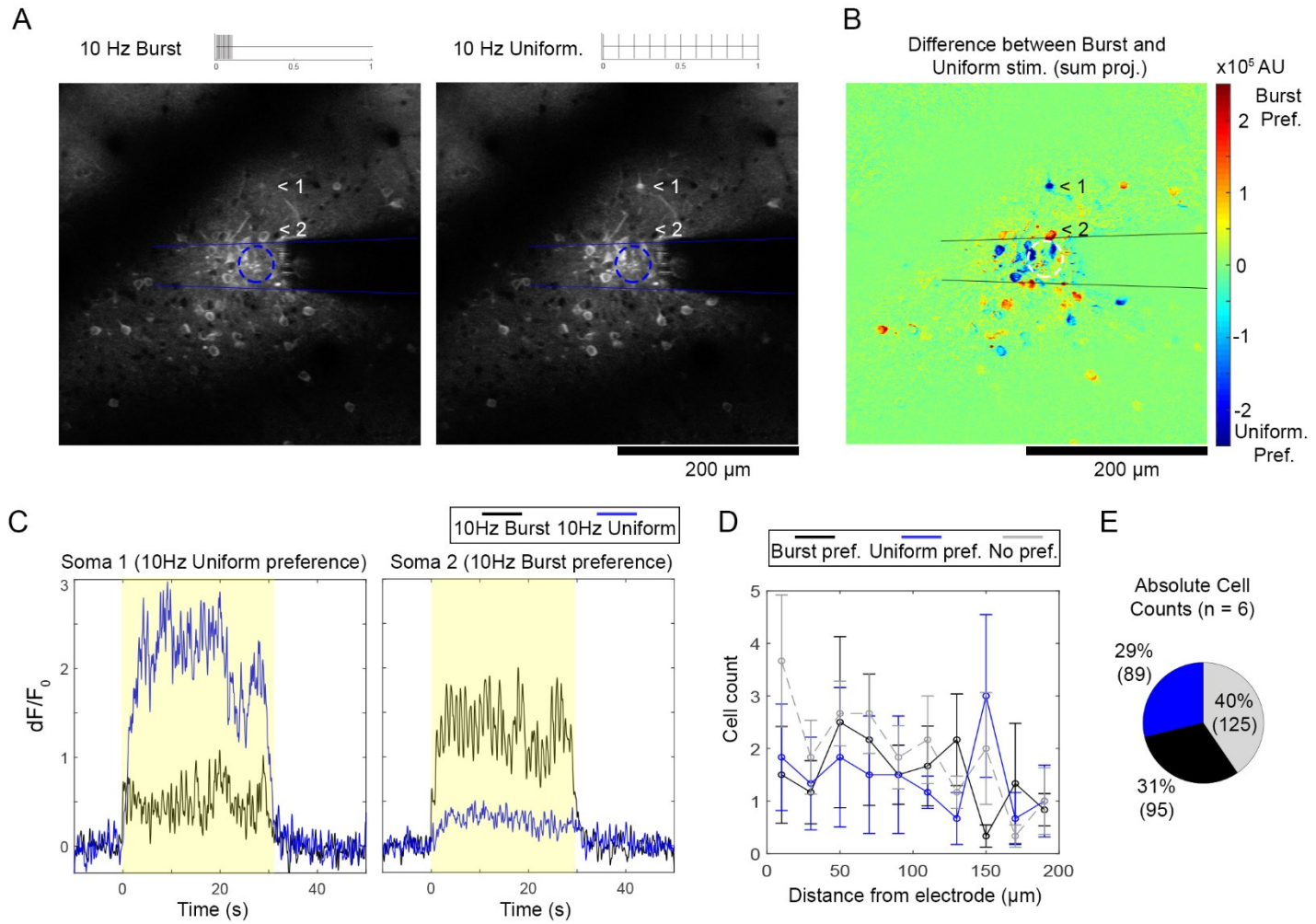


**Figure 2: Most neurons show a "preference" for either 10Hz-Burst or 10 Hz-Uniform TP that is not dependent on distance from the electrode.** A) Certain cells (for instance, cells indicated by 1 and 2) were active exclusively during 10Hz-Burst or 10 Hz-Uniform stimulation. B) The difference of the cumulative fluorescence over Burst and Uniform stimulations reveals cells with a preference for 10Hz-Burst with positive values (warmer colors) and a preference for 10 Hz-Uniform with negative values (cooler colors). C) Representative time traces for cells with 10Hz-Burst and 10 Hz-Uniform preferences indicated in A-B. D) "Preference" for TP was determined if the cumulative $dF/F_0$ for one pattern was 2X greater than the other. The distribution of cell counts over distance was similar between patterns ($p>0.05$). E) Pooled over all distances, the pie chart (right) shows roughly equal counts of cells that prefer Burst (31%) and Uniform patterns (29%), while 40% of cells preferred neither. All data presented as mean ± SEM. For this analysis, 309 cells were analyzed from n = 6 stimulation trials from a total of 5 animals.

Our positive control condition with 100Hz uniform stimulation and 10X total charge injection compared to the 10Hz patterns generally elicited much stronger neural responses (Figure 3). As in our previous reports, cells distant to the stimulating electrode failed to follow the 100Hz stimulation over the full 30 s stimulation train ([35, 44], Figure 4; Supplemental Movie 3). To account for this, comparisons between the 100Hz condition and the 10Hz conditions were confined to quantifying the first 2 seconds of stimulation (referred to as the onset period). During this period, the majority of cells 95.5% of cells either showed a preference for the 100Hz stimulation or no preference (Figure 3 A,C). Interestingly, 4.5% of cells preferred either 10Hz-Burst or Uniform stimulation (Figure 3B,C), with some cells showing an intense preference for the 10Hz-Burst condition (Figure 3D).

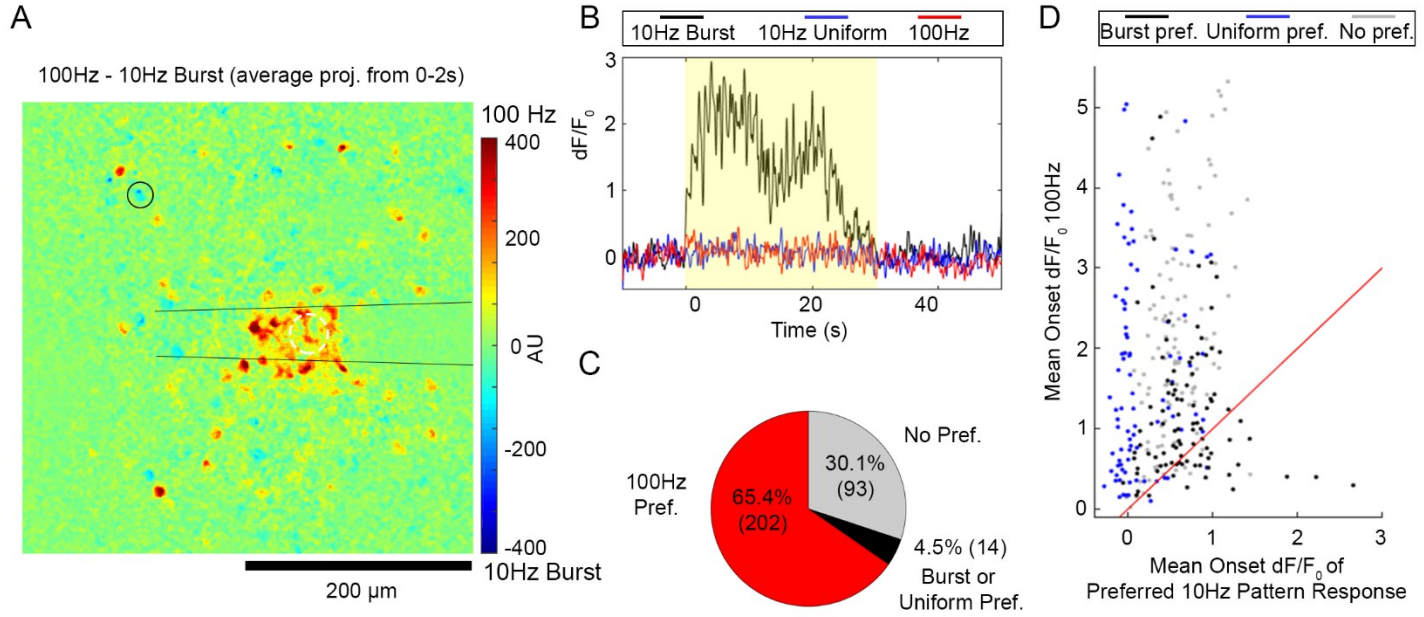


**Figure 3: Some neurons prefer 10Hz-Burst or Uniform stimulation to the 100Hz pattern despite 10X lower charge injection.** A) The difference of the cumulative fluorescence over 100Hz and 10Hz-Burst stimulations is projected such that cells that were more active during 100Hz had positive values (warmer colors) and cells that were more active during 10Hz-Burst had negative values (cooler colors). Some cells (example shown by the black circle) showed a slight preference for 10Hz-Burst relative to 100Hz. B) A time trace of a cell that preferred 10Hz-Burst over 10 Hz-Uniform and 100Hz patterns (cell indicated by the black circle in panel A). C) Cumulative counts of cells that preferred the 100Hz Pattern (red), preferred either 10Hz-Burst or Uniform over 100Hz pattern, or had no preference show that it is rare for a cell to not prefer the 100Hz pattern. D) Scatter plot where each point represents the mean $dF/F_0$ during the stimulation onset period (0-2s) for the 100Hz pattern (y-axis) and the highest mean onset $dF/F_0$ between 10Hz-Burst or Uniform. For this analysis, 309 cells were analyzed from n = 6 stimulation trials from a total of 5 animals.

Together, these results show that cells can exhibit a preference for certain temporal patterns that is not a function of distance from the electrode, and in a small fraction of cells is not a function of total charge injection. This begs the question: how does temporal pattern drive distinct spatial recruitment of neurons? In the subsequent sections, we test hypotheses that spatial recruitment is driven by cellular inactivation over long stimulation trains, excitatory neurotransmitter release patterns, and by changes in inhibitory-excitatory tone.

4.2. Bursting and Uniform 10Hz temporal patterns result in sustained temporal recruitment of neurons

Our previous work has indicated that stimulation frequency, amplitude, and square wave symmetry influence a cell's ability to follow a long stimulation train [35, 37, 44]. Given that cells distant to the electrode site fail to follow 100Hz positive control pattern over a 30 s train, we sought to determine if cells were able to reliably follow the 10 Hz-Burst condition, which contains 100ms bursts of 100Hz stimulation. However, we observed that most cells that were active during the 10 Hz-Burst or 10 Hz-Uniform stimulation followed the stimulation train compared to the 100 Hz stimulation (Figure 4A). We quantified the temporal aspects of the calcium response by isolating the time-course of GCaMP activity for 309 individual cell somas (examples in Figure 4B). To measure the temporal aspect of a neuron's activity, we used activation time—a measure of the uniformity of calcium expression in a cell through the stimulation period (Figure 4C). An activation time of 15 s indicates more uniform calcium activity through the duration of the stimulation, while <15s indicate that calcium activity was weighted toward the beginning of the stimulation (indicative of cells that are inactivated during the stimulation train), and >15s indicates that calcium was weighted toward the end of the stimulation (ie, the cell had higher fluorescence at the end of stimulation). Activation time for both 10 Hz patterns was significantly higher compared to the 100Hz pattern for cells close (≤60 µm) and far (>60µm) to the electrode (Two-way ANOVA significant effects for TP and distance $p<0.0001$; significant post-hoc tests indicated in Figure 4C). Further, activation time for close and far cells during both 10 Hz stimulations was similar, while there was a significant decrease in distant cells compared to close cells during 100Hz pattern stimulation ($p < 0.0001$). This ultimately shows that close cells maintained activation for the entirety of both 10 Hz stimulations, while many distant cells to the electrode failed to follow 100Hz stimulation.

We subsequently classified cells as either Onset (ON) if they were active during the first 0-2s of stimulation but not the entire 30s stimulation train, and Steady State (SS) if the cell was able to maintain calcium activity for the entire 30s stimulation train. In counts of ON and SS cells, there were significantly more SS cells for all TPs (Figure 4D, two-way ANOVA main effects for ON v. SS classification but not for TP: $p < 0.0001$). The mean $dF/F_0$ for SS cells was also elevated for all TPs (Figure 4E, two-way ANOVA main effects for ON v. SS classification and for TP: $p<0.0001$). SS cells in 100 Hz stimulation had a greater mean $dF/F_0$ than SS cells in either 10 Hz-Burst or 10 Hz-Uniform stimulation ($p < 0.0001$). The mean $dF/F_0$ measurement only considered $dF/F_0$ while the cell was active. Ultimately, this analysis shows that cells are able to follow stimulation pulses with an average frequency of 10Hz for long train for both TPs, while more cells tend to fail in following the 100Hz stimulation pattern.

While we observed that most cells sustained calcium levels during both 10 Hz-Uniform and 10 Hz-Burst TPs, calcium entrainment differed between the patterns (Figure 4B, F). This was evaluated by quantifying the relative 1Hz power during the different TPs. Because bursts occurred every second, 1Hz was the relevant frequency to track. Two-way ANOVA showed significant effects for TP and distance ($p < 0.00001$), with 10 Hz-Burst having higher 1Hz power than 10 Hz-Uniform or the 100Hz pattern at all distances ($p < 0.05$). Further, the 1Hz effect for 10 Hz-Burst was lower with distance from the electrode, with the most 1Hz power evident within 20μm of the stimulation site. While we anticipate that there should also be frequency-domain peaks at 10 Hz and 100 Hz, this could imply that the ‘off’ period is key to the 1 Hz power compared to 10 Hz power. However, the imaging rate of the 2P system and then biophysics of GCaMP are not conducive to tracking those frequencies [62]. These results together show that preferential activation of neurons during stimulations of different TPs is not due to cells failing to follow long trains of stimulation. Nonetheless, the temporal coding evident in the 1Hz power likely plays a role in shaping the neural response.

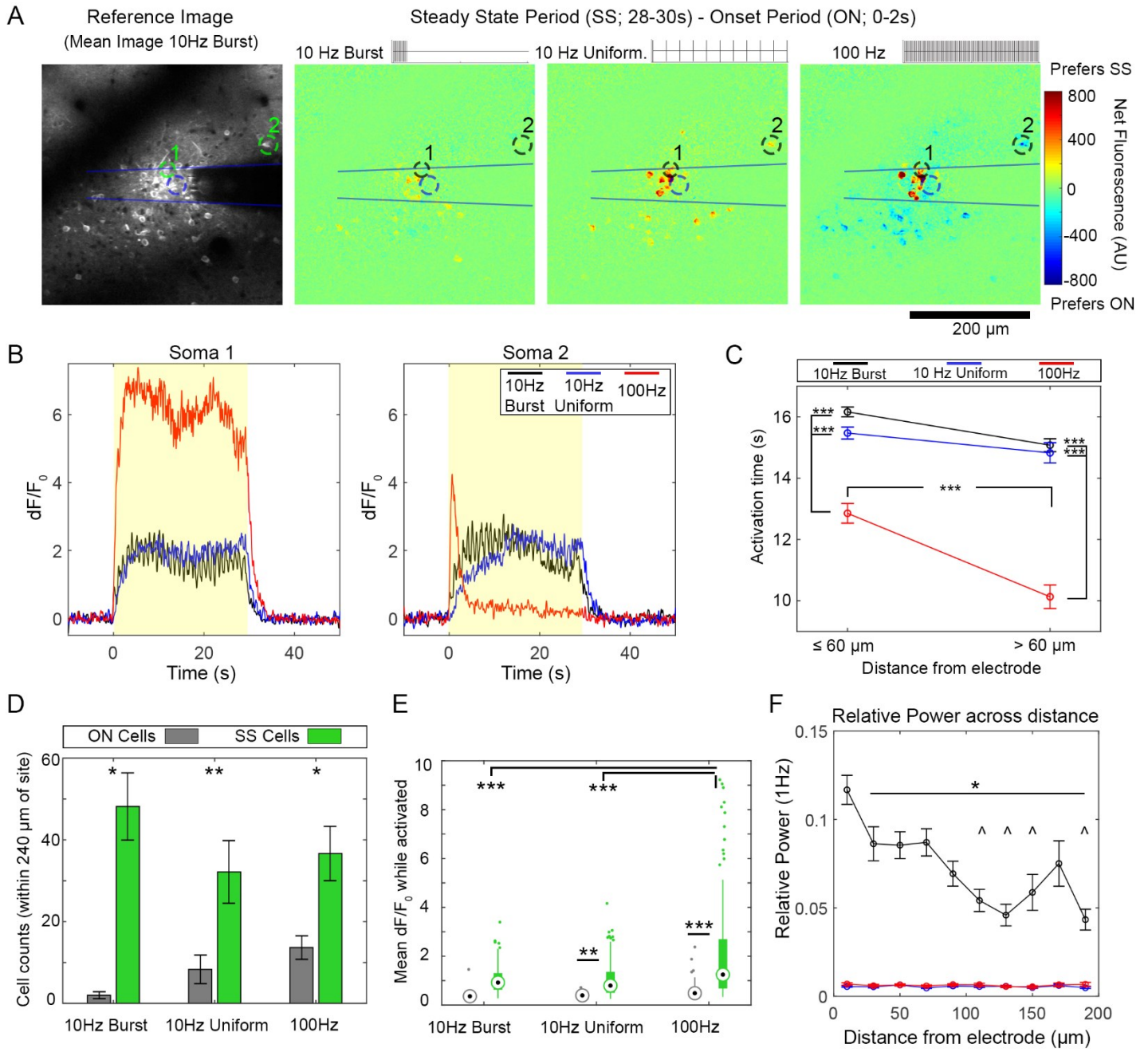


**Figure 4: Neurons have similar temporal responses to 10Hz-Burst and Continuous patterns while neurons tend to show more entrainment failure to the 100Hz pattern.** A) The difference in $dF/F_0$ between the Onset period (ON, 0-2s) and the Steady State period (SS, 28-30s) indicates how well neurons can follow a 30s train of each stimulation pattern. Increased activation during SS period compared to the ON period appears as a warmer color, while a decrease appeared as a cooler color. B) While many somas can stay active for the full stimulation train (Soma 1), some fail to follow the train (Soma 2, 100Hz) C) Activation time captures the ability of a cell to stay active during a stimulation train. Neurons respond similarly to 10Hz-Burst and Uniform patterns. In contrast with 100Hz pattern, cells show a reduced activation time (fails to entrain at a more rapid rate). Two-way ANOVA indicated a statistically significant effect for both pattern and distance ($p < 0.0001$) with post-tests showing that both 10Hz patterns had elevated activation time relative to 100Hz at all distances ($p<0.0001$). For the 100Hz stimulation, activation time was significantly reduced >60µm compared to ≤60µm ($p<0.0001$). D) There were more SS cells with all stimulation patterns (Two-way ANOVA significant effect for cell type ON v. SS: $p < 0.0001$) with * and ** indicating statistically significant post-hoc tests with $p < 0.05$ and $p < 0.01$, respectively. E) For mean $dF/F_0$, there were statistically significant effects between patterns and between ON v. SS cells (Two-way ANOVA, $p < 0.0001$). Post-hoc tests reveal that both 10Hz patterns had similar mean $dF/F_0$, while the 100Hz waveform had elevated SS mean $dF/F_0$ compared to the 10Hz patterns. SS cells had a significantly elevated mean $dF/F_0$ compared to the ON cells for the 10 Hz-Uniform and 100Hz as well (** and *** indicate $p < 0.01$ and $p < 0.0001$, respectively). E) Cells had significantly elevated relative 1Hz power during 10Hz-Burst stimulation compared to other patterns Two-way ANOVA analysis shows significant effects for stimulation pattern as well as distance ($p < 0.00001$), with elevated 1Hz power for

Burst stimulation compared to other groups at all distances ($p < 0.05$. Cells within 20 μm of the electrode had an elevated response to all other distances during Burst stimulation ($p < 0.05$). Cells at distances indicated by ^ were significantly elevated compared to cells within 40-80 μm of the electrode. Data in C,D, and E presented as mean ± SEM; data in D presented in box plots. For this analysis, 309 cells were analyzed from n = 6 stimulation trials from a total of 5 animals (6 hemispheres).

4.3. Excitatory neurotransmitter build-up is not observed during Bursting or Uniform 10Hz patterns

Section 4.2. suggests that while cells fail to follow uniform 100Hz stimulation after 1-5 seconds, they can easily follow 100Hz stimulation in 100ms bursts (10 Hz-Burst pattern). Brief bursts of high-frequency stimulation may also influence the reuptake of the excitatory neurotransmitter glutamate. Previous work has shown that prolonged high-frequency and high-amplitude stimulation can reduce glutamate reuptake, leading to build-up of the neurotransmitter in the extracellular space [35, 63]. If such a build-up was occurring during the 10 Hz-Burst pattern, it may explain the difference in spatial recruitment with different TPs. Using animals with viral expression of the glutamate sensor iGluSnFr under the control the hSyn promoter, we observed a patent glutamate build-up within 20μm of the electrode site during 100Hz stimulation, but not during either 10 Hz TP (Figure 5).

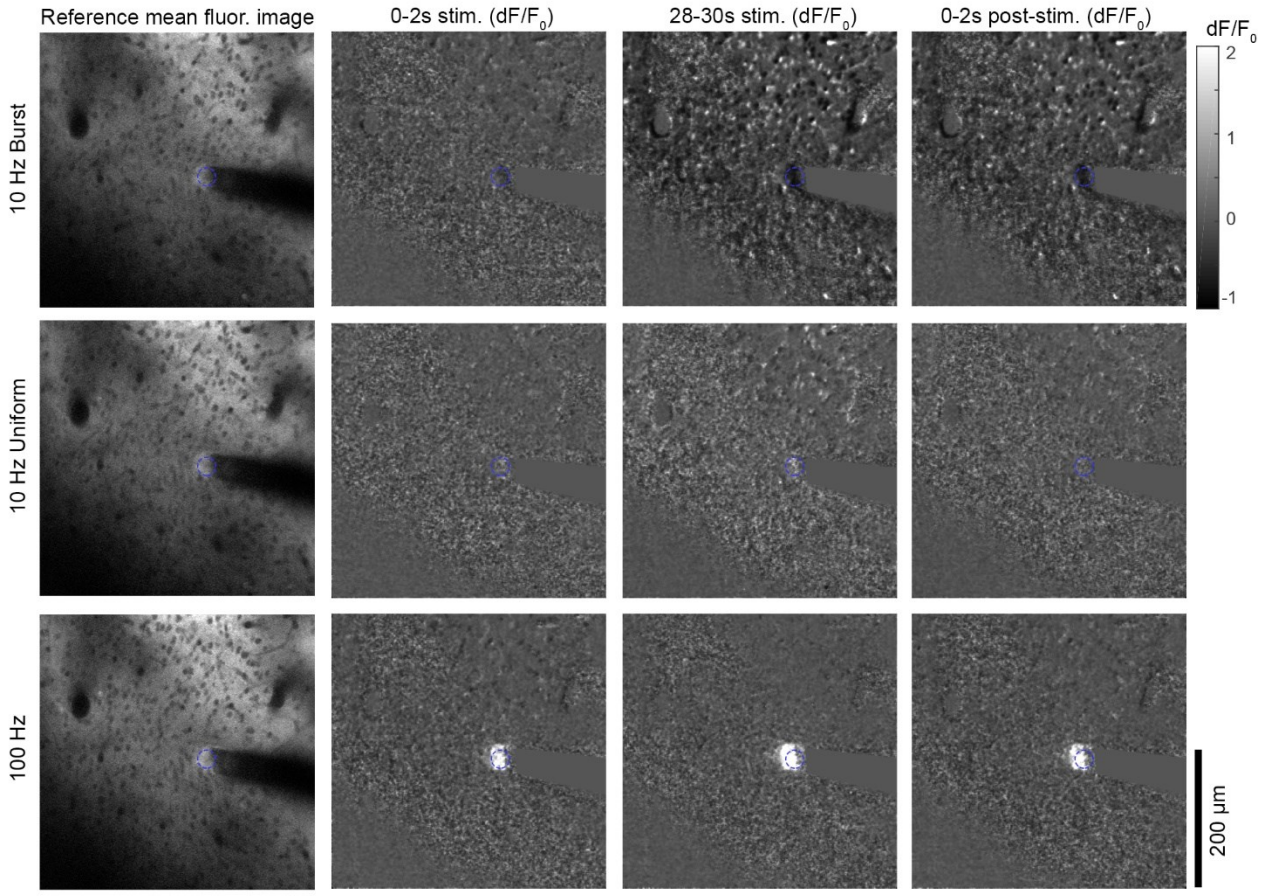


**Figure 5: Two-photon imaging glutamate release shows a pronounced response close to the electrode during the 100Hz stimulation, but not for either 10Hz pattern.** The glutamate response to ICMS was measured using the iGluSnFr transgene expressed in neurons under control of the hSyn promotor. The mean fluorescence of the baseline period is presented on the left for all stimulation patterns, while the mean $dF/F_0$ over the specified time periods is presented on the right for all stimulation patterns. The glutamate response is only detectable by eye for the 100Hz group. In all images, the electrode site is indicated by the blue dashed circle. See Supplemental Movies 3-6.

In observing the iGluSnFr $dF/F_0$ during stimulation, we noted that there was larger variation between animals, perhaps due to variable ketamine states throughout the experiments. Ketamine is known to target the

glutamatergic system, and may alter the iGluSnFr response during stimulation (Figure 6A) [64, 65]. Nonetheless, there was a consistent and statistically significant elevation of glutamate during the 100Hz stimulation, but not during either of the 10 Hz patterns (Figure 6B, two-way ANOVA significant main effects for TP and distance: $p < 0.0001$, with all indicated significant post-hoc tests $p < 0.0001$). Despite weak and variable responses during 10 Hz-Burst stimulation, there was an evident elevation in 1Hz relative power (Figure 6C) indicating that the 10 Hz-Burst stimulation was modulating glutamate activity. Two-way ANOVA showed a significant effect for temporal pattern ($p < 0.001$), but not distance and with no significant post-hoc comparisons. In parity with section 4.2., these results indicate that excitatory neurotransmitter release is similar during both 10 Hz temporal patterns, though the bursting activity is evident in neural response to 10 Hz-Burst activity.

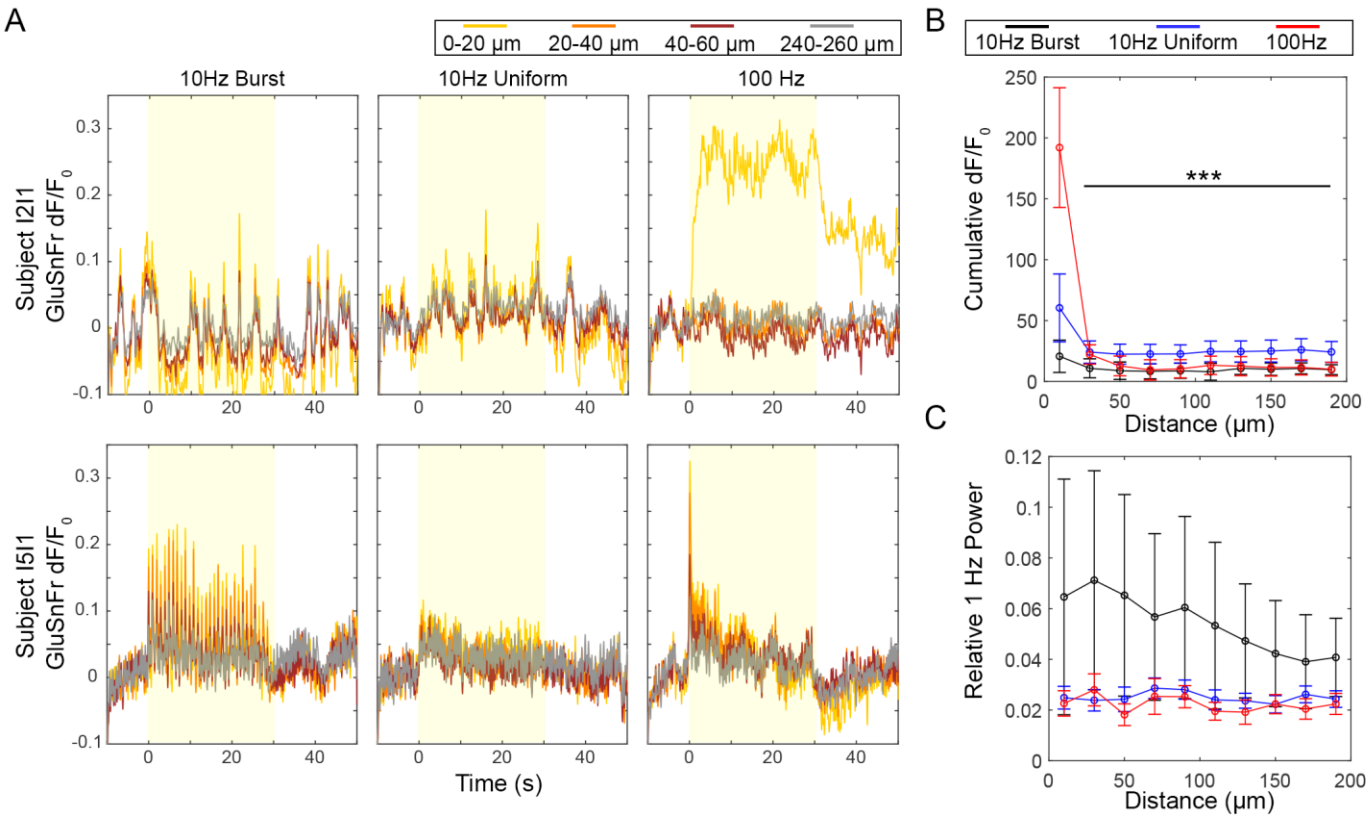


**Figure 6: Glutamate release is elevated close to the electrode during the 100Hz pattern, but there is also detectable glutamate release during 10Hz-Burst stimulation.** A) Representative traces from two stimulation trials in two subjects. Subject I2I1 shows strong response during the 100Hz pattern, but little response during either 10Hz pattern. Subject I5I1 shows a strong response during Burst stimulation with apparent entrainment during 1Hz-Bursts. The subject likewise shows some response during 10 Hz-Uniform and 100Hz patterns. B) The cumulative $dF/F_0$ indicates that the strongest glutamate response was for the 100Hz pattern within 20µm of the electrode. Two-way ANOVA yielded significant effects for pattern and distance ($p < 0.0001$) with post-hoc tests indicating a significant increase for the 100Hz pattern at within 20µm of the electrode and all other patterns and distances ($p < 0.0001$). C) For some subjects, there was strong glutamate entrainment to 10Hz-Bursting as shown by an elevated 1 Hz power. This was confirmed by a Two-way ANOVA, which showed a statistically significant effect for pattern ($p<0.001$). Due to the high variance in the data, there were no significant post-hoc tests. Data in B and C presented as mean ± SEM. n = 7 trials from a total of 4 subjects.

### 4.4. Inhibitory-excitatory tone during stimulation may underlie cell preference for temporal pattern

In the previous experiments we show that TP influences the frequency of the calcium and glutamate responses during stimulation. Otherwise, cells that are active during 10 Hz-Burst and 10 Hz-Uniform stimulation have similar temporal characteristics. How can this expected result explain our initial observation that temporal pattern yields distinct spatial recruitment of neurons? To address this, we need to infer the activity of a cell population that is not widely observable with the *Thy1*-GCaMP model: inhibitory neurons. Layer II/III of the sensory cortex is hallmarked by its dense inhibitory connections [60]. Single-neuron stimulation and modeling experiments have shown that pyramidal cell bursting (largely what is observed in the GCaMP model) yields

greater correlation in output activity that results in greater inhibitory cell recruitment and downstream changes in the inhibitory-excitatory balance of the sensory cortex [61, 66, 67]. Bursting and output correlation are also implicated in awake v. anesthesia states, where somatic neural activity in the awake cortex is less correlated to the neuropil activity compared to anesthetized states [68-70]. These studies suggest that the spatial correlation between the 99% excitatory somatic neural activity and neuropil neural activity is intertwined with the inhibitory-excitatory tone of the cortex. To quantify this relationship during TP stimulation, we isolated the neuropil calcium signal from our time-series images by masking out the somas (Figure 7). The mean neuropil activity in 20μm bins radiating from the electrode site was quantified as a function of time (Figure 7A). To capture potential failure of the neuropil to follow the stimulation train, we quantified the difference of the mean Steady State $dF/F_0$ (28-30s of stimulation) and the mean Onset $dF/F_0$ (0-2s). Similar to the somatic response, the 100Hz pattern resulted in significantly more loss of calcium activity in the neuropil (Figure 7B, two-way ANOVA significance for TP and distance: $p < 0.0001$, with significant pairwise comparisons indicated). The correlation was measured between any a given soma and the corresponding neuropil bin as depicted in Figure 7C. There were statistically significant effects for both TP and distance on the Soma-Neuropil correlation (Figure 7D; two-way ANOVA, $p < 0.0001$), with post-hoc tests showing that the 10 Hz-Burst and 100Hz TPs had significantly elevated correlation compared to the 10 Hz-Uniform group. For all groups, there was a decline in correlation with distance from the electrode. Beyond 60 μm from the electrode, differences between the 10 Hz-Burst and 100 Hz TPs became apparent, with significantly elevated correlation for the 10 Hz-Burst TP.

While these soma-neuropil correlation results alone show that the 10 Hz-Burst altered the interplay between neuropil and somas, we can further tie these results back to cellular preference (Figure 2). Cells that preferred 10 Hz-Burst had higher soma-neuropil correlation during 10 Hz-Burst stimulation compared to cells that preferred 10 Hz-Uniform stimulation (Figure 7E; two-way ANOVA $p < 0.001$). There was no difference in soma-neuropil correlation during 10 Hz-Uniform stimulation for cells with different preferences. This shows that cell preference is influenced by a cell's relationship to the surrounding neuropil.

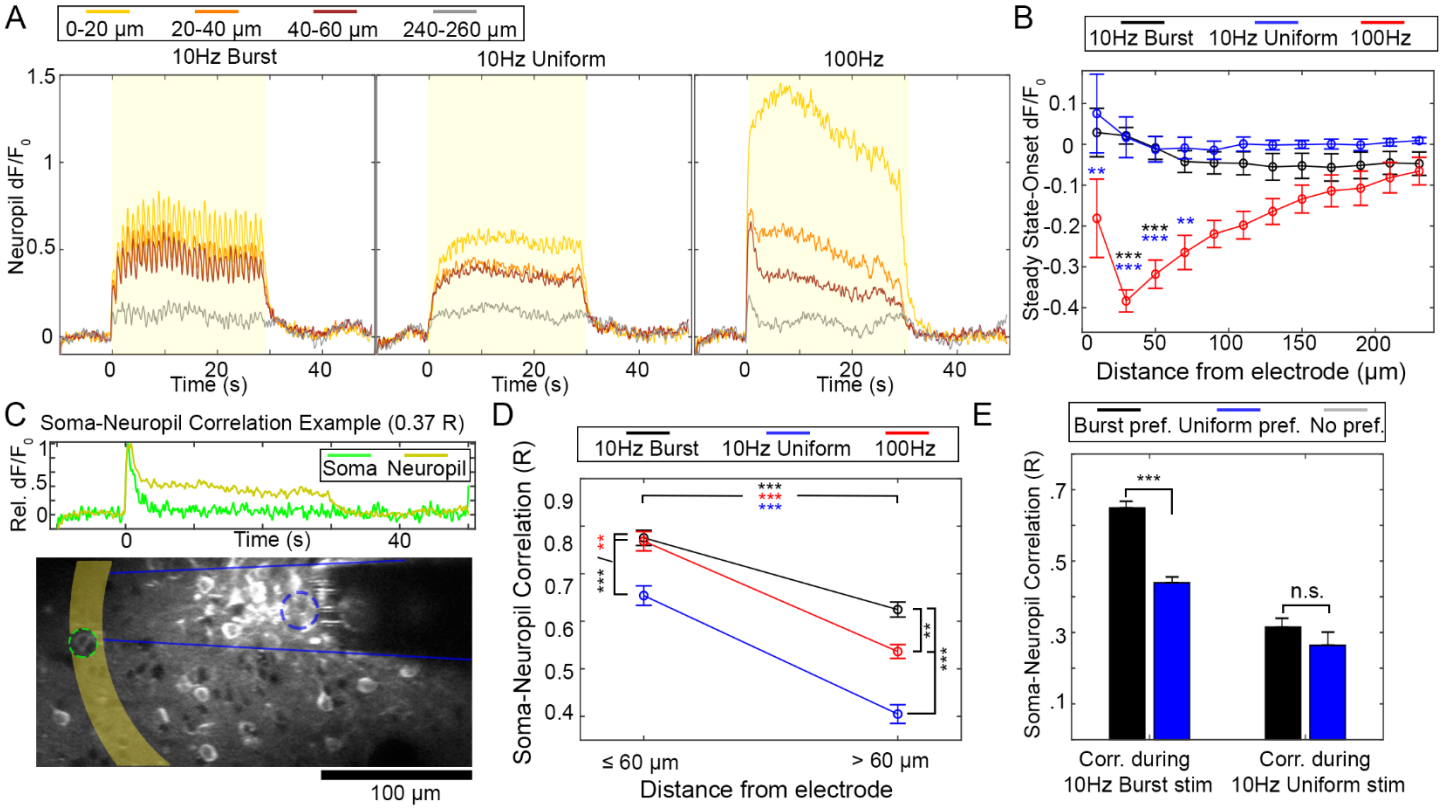


**Figure 7: Neuropil calcium activity is highly correlated to somatic calcium activity during 10Hz-Burst and 100Hz stimulation, but significantly less so for 10 Hz-Uniform stimulation.** A) Representative $dF/F_0$ from the neuropil as a function of time for each stimulation pattern. Color represents different distances from the electrode array. The stimulation period is indicated by a yellow box. B) Like the somatic response to 100Hz pattern but not for either 10Hz pattern, calcium activity faded between the Onset period and Steady State period. A two-way ANOVA indicates that there was a statistical difference between stimulation pattern, but not distance, with post-hoc tests indicating that the 100Hz group experienced

significantly more $dF/F_0$ loss compared to the 10Hz patterns as indicated by the black and blue *, with ** indicating $p < 0.01$ and *** indicating $p < .0005$. C) The correlation between calcium in a soma and the neuropil within the same distance bin can be calculated. D) The Soma-Neuropil Correlation was modulated by temporal pattern. Namely, 10Hz-Burst and 100Hz stimulation patterns had elevated soma-neuropil correlation proximate and distant to the electrode site relative to the 10 Hz-Uniform pattern. Two-way ANOVA showed a statistically significant effect for both pattern and distance ($p < 0.0001$), with post-hoc tests indicating that correlation was reduced for all groups at >60 μm compared to ≤60 μm. Further, somas and neuropil were more correlated with 10Hz-Bursting and 100Hz patterns than with 10 Hz-Uniform stimulation at all distances. ** and *** indicate $p < 0.01$ and $p < 0.0001$, respectively. E) Soma-neuropil correlation during 10Hz-Burst stimulation was significantly elevated for cells that preferred 10Hz-Burst stimulation compared to cells that preferred 10 Hz-Uniform stimulation (Two-way ANOVA and post-hoc tests: $p < 0.001$). However, correlation during 10 Hz-Uniform stimulation as similar between cells of both preferences. All data presented as mean ± SEM. For this analysis, 309 cells were analyzed from n = 6 stimulation trials from a total of 5 animals.

Cell preference is related to soma-neuropil correlation, which in turn is known to be related to inhibitory-excitatory tone. Neural inhibition may be detected as a negative value in GCaMP $dF/F_0$. While we observed few instances of negative $dF/F_0$ under the 2P microscope, we also examined the calcium response to TP stimulation with under a mesoscale, fluorescence microscopy rig (Figure 8). This enabled imaging across the entire craniotomy area. Due to the lower axial resolution of the fluorescent light source, the signal observed in these studies captured calcium activity through multiple depths of the cortex as well. In mesoscale imaging, we noted that both 10 Hz TPs resulted in focal neural activation at the electrode site that persisted throughout the stimulation train, while the 100Hz pattern had a much stronger initial neural activation that diminished over the 30 s train (Figure 8A). This was consistent with our previous reports in this model [35, 44]. Similar to the 2P results, there was a decline in $dF/F_0$ between the SS and ON period (Figure 8B, two-way ANOVA effect for TP: $p <0.001$). To quantify any negative $dF/F_0$ activity, we collected the mean $dF/F_0$ over the 30s stimulation period and measured the mean fluorescence in 60 μm bins radiating out from the electrode site (Figure 8C). Two-way ANOVA showed that there was a statistically significant difference across temporal patterns and across distance from the electrode ($p < 0.0001$). Post-hoc tests confirmed that 100Hz pattern generated a higher $dF/F_0$ close to the electrode site (0-60μm) compared to the 10 Hz-Burst group. Post-hoc tests also confirmed that mean $dF/F_0$ at 0-60 μm was significantly higher than 300-660μm for 10 Hz-Burst ($p < 0.05$) and higher than 150-1000μm for the 100Hz pattern ($p < 0.001$). Importantly, both 10Hz TPs showed slight inhibition effects beyond 180μm from the electrode. This suggests that temporal pattern can drive inhibition in a distance-based manner.

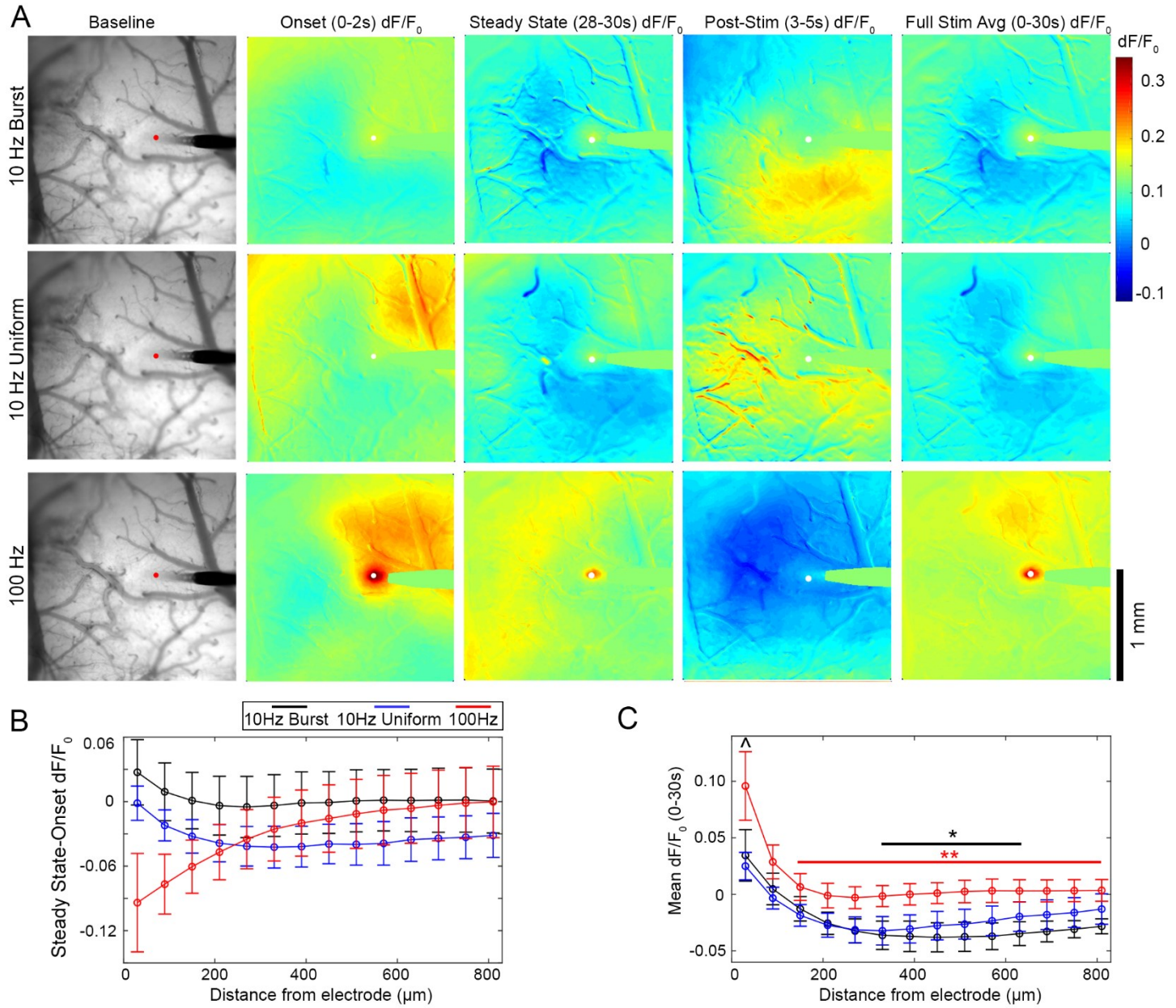


**Figure 8: Mesoscale imaging of neuronal calcium response to ICMS shows distant inhibition during both 10Hz patterns.** A) Representative images of the neuronal calcium response to 10Hz-Burst and Uniform stimulation patterns. Images are shown as an average of fluorescence intensity over the baseline period, the $dF/F_0$ from 0-2s of stimulation, 28-30s of stimulation, and 3-5s post-stimulation, and the mean $dF/F_0$ over the entire 30s stimulation train. See Supplemental Moves 7-9 for activation over time. B) Similar to the two-photon neuropil imaging, there is loss of activity over the 30s stimulation train proximal to the electrode for 100Hz stimulation. Interestingly, there in regions beyond the 2P imaging window (>250μm), there was also loss of activity for over the stimulation train for both 10Hz groups (significant two-way ANOVA effect for temporal pattern: $p < 0.001$). C) Further, mean $dF/F_0$ over the stimulation train (0-30s) as a function of distance from the electrode shows distant inhibition for both 10Hz stimulation patterns., but not the 100Hz pattern. Two-way ANOVA confirms that there is a statistically significant difference between the patterns and over distance ($p < 0.0001$), with ^ indicating a significant difference between the 10Hz-Burst pattern and 100Hz patterns within 0-60 μm of the electrode ($p< 0.05$). Additionally, * and ** indicate significant differences between the 0-60 μm bin and indicated bins ($p < 0.05$, $p< 0.001$, respectively. Color indicates the pattern of comparison). Data is presented as mean ± SEM, with n = 4 stimulation trials from a total of 3 different animals.

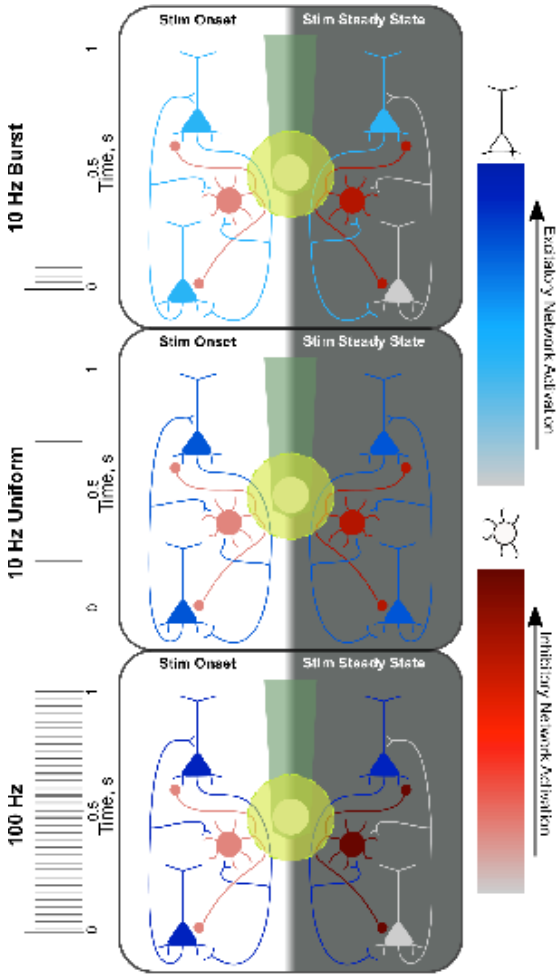


**Figure 9: Temporal pattern of stimulation differentially drives excitatory and inhibitory network activation.** Electrical stimulation directly activate neuronal fibers passing through the ~20 um radius around the electrode (yellow circle) and antidromically activating associated neuronal soma. At the same orthodromic activation of passing axons post-synaptically activate downstream neurons (indirect electrical stimulation activation) and the relative drive of the excitatory and inhibitory networks. During the onset period of all TPs, inhibitory network activation is low, with 10Hz-Burst having the lowest excitatory neuronal activation due to the pyramidal neurons' absolute refractory period extending through the majority of the burst duration. Network inhibition builds during all TPs leading to inactivation of neurons activated orthodromically (*i.e.* indirect activation, trans-synaptic activation). Because excitatory neurons outnumber inhibitory neurons, the excitatory drive onto orthodromically activated neurons outweighs the inhibitory drive leading to more stable activation. (See Figure S1 for extended version).

## 5. Discussion

Accurate control over the temporal rate code of neurons is essential for artificial touch. The frequency of stimulation has been shown to not only modulate the intensity of artificial perception, but also the quality perception in nonhuman primates [10, 17]. These studies on frequency all use a uniform distribution of stimulation pulses. This distribution or spacing of stimulation pulses over a train—or Temporal Pattern (TP)—presents as another little-understood parameter space of therapeutic interest [22]. The average firing rate does not sufficiently describe sensory processing; therefore, one aim of using TPs in stimulation of the nervous system is to precisely control the rate code of neural activation to more accurately mimic physiological patterns of neural activity (eg. biomimetic stimulation). However, while TP has been used to modulate the quality of perception in ICMS and to relieve symptoms in Parkinson's disease, there are few mechanistic studies explaining why [71].

The main findings of the present work are that temporal patterning in ICMS leads to distinct patterns of cortical neural activation (Fig. 1-3, 7-8). However, temporal patterning of ICMS also sheds light on the mechanisms

underlying neuronal recruitment via ICMS and inform engineering designs of biomimetic stimulation pulse patterns from an infinite stimulation parameter space. Using mesoscale and two-photon fluorescence imaging of the calcium activity in *Thy1* cortical neurons, we demonstrate that neurons show similar temporal activation responses to temporally patterned ICMS containing the same amount of cumulative charge injection and same average frequency of 10 Hz, but with pulses either delivered uniformly (10 Hz-Uniform: 1 pulse every 100 ms) or in bursts (10 Hz-Burst: a 100ms burst of 10 pulses every second). Specifically, we observed that altering the temporal pattern of stimulation could drive distinct neural network activity, with a majority (60% of 309 quantified cells) of responsive neurons being preferentially activated by either the 10 Hz-Burst or 10 Hz-Uniform stimulation. The discrepancy in spatial activation pattern could not be captured by a simple distance relationship from the electrode site. Despite the unique spatial patterns of recruitment, both 10 Hz-Burst and 10 Hz-Uniform stimulation resulted in similar and stable temporal recruitment of neurons proximal and distant to the electrode site during a 30s train, while distant cells activated by a 100Hz stimulation pattern were more likely to fail in staying active for the 30s train. In addition, the three stimulation patterns did differ in their synchronous recruitment of somatic and neuropil elements—the 10 Hz-Burst condition resulted in significantly higher correlation between the neuropil and somatic compartments compared to the 10 Hz-Uniform condition, which could be responsible for specific stimulation preference. Paired with mesoscale and 2-photon iGluSnFR imaging, our results indicated distal inhibition in both of the 10Hz average frequency TPs ultimately suggest that temporal patterning drives distinct network activity by affecting the delicate inhibitory-excitatory balance that governs cortical Layer II/III [60]. These results have implications in the use of different temporal patterns for therapeutic applications of biomimetic stimulation, but also highlight the importance of better understanding the mechanisms of electrical microstimulation and the diversity of cell types involved.

### 5.1. Temporal Patterns on network inhibition during ICMS.

Temporal patterning of ICMS leads to spatially independent preferential activation of specific neural populations (Fig. 1-3) which appears to be a product of differential control over network inhibition (Fig. 8, 9). Widefield epifluorescent 1-photon GCaMP imaging enables examination of the broader neural network affects over a greater region of cortex compared to two-photon imaging. At the onset of the stimulus, there is broad activation around the electrode that decreases with distance. As the stimulus pulse train continues, 10 Hz-Burst and 10 Hz-Uniform show decreased neural activity up to 1 mm from the stimulation site. While some resting state oscillation can be seen over the imaged cortical region [72], these oscillations appear to display depressed activity as they pass through cortical regions influenced by ICMS (See Supplemental Movies 7-9). This effect can be more easily observed when an average intensity projection is made over the full 30 second stimulation duration (Fig. 8A,C). Interestingly, over the 30-s stimulation period, 10 Hz-Burst and 10 Hz-Uniform display similar activation and inhibition profiles within 300 μm, 10 Hz-Burst led to significant GCaMP inhibition from 300-650 μm in contrast to 10 Hz-Uniform, which did not. This observation begins to make sense when considering the excitatory and inhibitory neuronal composition of Layer II/III of sensory cortex, which consists of ~80:20 excitatory to inhibitory ratio [73-77]. In the model used in this study, the *Thy1*-GCaMP expression is predominantly in excitatory cells, but ~1% of *Thy1*-GCaMP cells are inhibitory cells (GAD67+) [78]. In the cortex, excitatory neurons are typically responsible for propagating information across the laminar layers [79] and generally entrain at frequencies below 8-10 Hz [80]. In contrast, Layer II/III inhibitory neurons can entrain or phase lock at higher frequencies and play a more diverse role in sensory cortices, including lateral inhibition, response modulation and network stabilization [38, 81-84]. Therefore, it is possible that the 100ms bursts of 100Hz stimulation in 10 Hz-Burst can drive more inhibitory cell firing relative to excitatory cell firing compared to 10 Hz-Uniform. Together, these facts begin to shed light on the underlying mechanisms that lead to distinct neural activation patterns from temporal patterned ICMS.

Inhibition plays a critical role in shaping the temporal response to electrical stimulation [30, 31]. Specifically, without lateral inhibition, the duration and spatial spread of activation is significantly increased [30, 31]. Therefore, it is not surprising to observe an inhibitory network response during long duration high frequency or patterned stimulation. The 10 Hz-Burst and 10 Hz-Uniform results highlight a similar activation pattern within 300 μm from the electrode site as observed by widefield one-photon GCaMP imaging (Fig. 8A,C; Supplemental movies 7-9), somatic GCaMP activity (Fig. 1,4; Supplemental Movies 1-3), and neuropil activity (Fig. 7). However, there are some distinct differences between 10 Hz-Burst and 10 Hz-Uniform.

Fast spiking and burst-spiking inhibitory neurons can entrain to higher frequency stimulation [77]. Since, 10 Hz-Burst stimulation is best suited to entrain these classes of inhibitory neurons (100 ms bursts of 100 Hz), it is expected that 10 Hz-Burst leads to stronger inhibitory oscillations compared to 10 Hz-Uniform (Fig. 8A,C). 10 Hz-Burst likely accumulates inhibitory network effect with bursts of consecutive pulses at 100 Hz that drives multiple action potentials in some inhibitory neurons for each excitatory neuronal activation (Fig. 9; Fig. S1). In fact, single-cell stimulation studies have shown that bursts of at least 5 APs in layer II/III pyramidal cells are necessary to reliably recruit downstream interneurons, and a burst frequency range between 25-100Hz is necessary to reliably alter cortical up/down states [61, 66]. The 10 Hz-Burst stimulation used in this study fits within that criteria, and may explain why distinct spatial recruitment was observed. Furthermore, $GABA_B$ receptor activation is more prominent after high frequency stimulation, which could increase the duration of inhibitory control during 10 Hz-Burst [85, 86]. Importantly, the balance of excitatory and inhibitory input onto neurons significantly impacts the activation probability of both the axon and the soma [87]. This build-up of the inhibitory neural network likely leads to a greater overall suppression of excitatory neurons over the 900 ms break for 10 Hz-Burst and, in turn, results in an overall average inhibition over the 30 s stimulation duration [88]. This can explain why there is no significant difference between the activation of steady state and onset cells compared to 10 Hz-Burst (Fig. 4E).

On the other hand, 10 Hz-Uniform provides a better understanding of the inhibitory and excitatory balance. Since more excitatory neurons can entrain at 8-10 Hz [80], each 10 Hz-Uniform pulse activates a more equally weighted balance of excitatory and inhibitory neurons (Figure S1, Figure 9). Because the number of excitatory neurons outweigh inhibitory neurons in the cortex[89], the activation of inhibitory neurons is likely to reduce the activation of some excitatory neurons, but overall excitation is expected to dominate. This is likely why elevated calcium activity of steady state neurons was observed for 10 Hz-Uniform compared to onset neurons (Fig. 4E). The iGluSnFr data further supports the hypothesis that temporal pattering influences inhibitory-excitatory tone by showing less glutamate release for 10 Hz-Burst compared to 10 Hz-Uniform (Fig. 5,6; Supplementary Movies 4-6). Identifying the neuronal subtype for neurons displaying unique preferences to each temporal pattern will enable a better understanding of the underlying mechanism.

### 5.2 Temporal Patterning on excitatory neurons during ICMS

If the 100 Hz at 10% temporal pattern (10 Hz-Burst) leads to a greater inhibitory network effect, it might be expected that longer durations of 100 Hz (100% temporal pattern) would lead to even greater inhibition. In fact, suppression of neural activity may be a critical component of the therapeutic profile of high frequency stimulation in DBS [90]. Despite this, we observe that the 100 Hz stimulation pattern leads to significantly greater GCaMP activity (Fig. 3,4,8; Supplementary Movies 1-3, 7-9). This is also supported by the iGluSnFr data, which shows significantly elevated glutamate release during 100 Hz stimulation compared to 10 Hz-Burst and 10 Hz-Uniform (Fig. 5,6; Supplementary Movies 4-6). It should be noted that glutamate uptake rate is regulated by the firing frequency, therefore iGluSnFr activity cannot be used to estimate the activation frequency of excitatory neurons [63, 91]. These two observations suggest that the greater iGluSnFr activity implies greater excitatory network activation. Another interesting observation is that an iGluSnFr 1 Hz activity was observed for 10 Hz-Burst stimulation, despite having the lowest iGluSnFr fluorescence overall (Fig. 6C). This again suggests that there is a strong excitatory activation at the onset of each burst with 10 Hz-Burst. However, the high frequency burst and 900 ms break leads to overall greater suppression. It remains to be investigated if the preferential proximity of the electrode site to predominately excitatory or inhibitory neuronal elements is the leading source of this variability. Variability in axonal geometry and proximity to the electrode could influence the activation probability and entrainment efficiency and explain frequently observed variability in stimulation efficacy or performance [87, 92, 93]. Nevertheless, for 10 Hz-Burst, this 1 Hz power can also be observed in steady state soma and neuropil activity, which provide additional insights into how ICMS temporal patterning influences the balance of excitatory and inhibitory networks.

The localization of glutamate release observed in this study may also explain the increased excitation observed during 100Hz stimulation. As in our previous work , we demonstrate that direct electrical stimulation at 100 Hz leads to significant glutamate release in a highly localized volume of tissue (< 20 μm) surrounding the microelectrode site (Fig. 6; Depicted by yellow circle Fig. 9, Fig. S1) [33]. In turn, this suggests that electrical stimulation only drives antidromic activity for axons that pass through this small region (Fig. 9) or alternatively, orthodromic activation for neurons with sufficient levels of dendrites or soma surface area within

this activation volume, or post-synaptic activation [94, 95]. For excitatory neurons with highly excitable neuronal elements (e.g., the axon initial segment [96]) within the direct activation volume, they are likely to fire an action potential at the onset of the stimulation pulse train. However, because excitatory neurons cannot generally entrain to extracellular stimuli beyond 10-15 Hz stimulation [80], the following pulses are not likely to generate action potentials in these excitatory neurons leading to low excitatory network drive (Fig. 9; Fig. S1). This is because high frequency stimulation can lead to buildup of extracellular potassium, which can increase [97] or decrease the excitability of neuronal elements leading to axonal block [96, 98]. Nevertheless, because the 100 Hz stimulus is uniform, as soon as an excitatory neuron's absolute refractory period ends, there is an immediate stimulation pulse that follows within 10 ms, which may explain the sustained GCaMP excitation seen in wide-field imaging (Fig. 8). However, 3-5 s post stimulation, there is a strong inhibition of GCaMP activity, suggesting a strong lasting inhibitory effect (Fig. 8A). Furthermore, inhibitory neurons are also receiving depressing input from the inhibitory network activation, which, over time, could reduce the balanced inhibition [99]. In turn, this leads to an overall greater GCaMP activity in neurons with neuronal elements in the direct activation volume regardless of excitatory or inhibitory identity.

**5.3 Temporal Patterning on inhibitory-excitatory network balance**

The balance of excitatory and inhibitory networks is influenced by temporal patterning of ICMS (Fig. 8,9). 10 Hz-Burst leads to a robust 1 Hz excitatory activation followed by a strong inhibitory network effect. In contrast, 10 Hz-Uniform leads to a more balanced activation of both excitatory and inhibitory networks. In turn, 10 Hz-Burst and 10 Hz-Uniform provide important evidence of the underlying properties of excitatory and inhibitory networks during ICMS. Specifically, with 10 Hz-Burst, the 1 Hz power in iGluSnFr activity (Fig. 6C) and somatic GCaMP activity (Fig. 4F) suggest that a substantial portion of the accumulated inhibitory network activity in the 100 ms burst washes out over the 900 ms rest (Fig S1.). Despite this strong 1 Hz excitatory effect, there is, on average, an overall inhibition to the network, which can be seen in the widefield GCaMP imaging data (Fig. 8). The strong inhibitory network activation, washout period of inhibition, and strong 1 Hz excitation may explain the high soma-neuropil correlation at distant locations (Fig. 7D). Specifically, while some groups have observed independent calcium dynamics between the soma and neuropil [68, 69], the timing of the excitation and inhibition in response to 10 Hz-Burst allows a stronger coordination of soma and fiber activation especially considering entrainment dynamics differ between the soma and axon at higher frequencies [87], which can lead to different populations of neurons preferring one TP over another (Fig. 1,2).

In contrast, while the widefield GCaMP imaging suggests similar levels of excitation and inhibition between 10 Hz-Burst and 10 Hz-Uniform near the electrode site (Fig. 8), two-photon imaging reveals that 10 Hz-Uniform has significantly lower soma-neuropil correlation compared to both 10 Hz-Burst and the 100Hz pattern (Fig. 7D). Interestingly, lower soma-neuropil correlations are more indicative of awake, baseline states with normal levels of inhibitory-excitatory balance [70]. This experimental evidence supports a theoretical relationship between soma-neuropil correlation and inhibitory-excitatory balance. Inhibitory post-synaptic potentials sum in the dendrites and soma [100, 101]. Therefore, in an inhibited state, the neuropil (largely composed of axons) may show elevated calcium activity, while inhibitory post-synaptic potentials may cause diminished somatic calcium activity, resulting in a low soma-neuropil correlation (as seen in Figure 7C). Modeling studies further corroborate that bursting activity can drive increased output correlation, which is in turn, effective in modulating up-down states within the cortex [61, 67]. Given that we saw that cell preference for 10 Hz-Burst v. 10 Hz-Uniform had a statistically significant relationship with soma-neuropil correlation during 10 Hz-Bursting activity, it is plausible that Bursting was effective in driving correlated states that influenced the inhibitory-excitatory tone of the cortex. In addition to this, we do not observe a discernible 10Hz power increase during 10 Hz-Uniform stimulation, which could suggest that there is no comparable "wash-out" effect as observed for 10 Hz-Burst and thus more of an inhibitory-excitatory balance. While this is a tempting interpretation, it should be noted that the slow kinetics of the GCaMP6s makes it unlikely to detect 10Hz phenomena [62]. Future studies could address this by using the faster GCaMP6f or GCaMP3 calcium sensors [102]. Nonetheless, as we know that both inhibitory and excitatory cells can follow 10Hz stimulation [80], it is plausible that both cell types are actively contributing to the inhibitory-excitatory balance (Fig. 9).

In previous GCaMP neuropil evaluation with 100 Hz stimulation, it was demonstrated that a substantial portion of neurites were being activated throughout the stimulation train and that the neuropil activity was strongly correlated to the steady state neuron activity [33]. This suggested that that ICMS likely led to inhibition of onset

neurons rather than conduction failure or hyperpolarization. While substantial work describing and characterizing virtual anode effects were carried out in cardiac defibrillation research [103], it should be noted that this effect decreases as the electrode size, pulse width, amplitude, and threshold decreases as in the case of ICMS. Therefore, it would not be surprising that an increased inhibitory drive onto indirectly activated neurons is responsible for the onset effect (Fig. 9; See Section 5.4).

As described earlier, 100 Hz stimulation leads to the greatest level of both excitatory and inhibitory network activation, because even if the neurons are unable to entrain to the stimulus, as soon as the neurons are ready to firing another action potential, there is an immediate depolarizing stimulation pulse that arrives within 10 ms. The excitatory influence of this stimulation can be observed in the level of glutamate release compared to 10 Hz-Burst and 10 Hz-Uniform (Fig. 5-6, Supplementary Movies 4-6). Given the 75~80% excitatory neuron to 25~20% inhibitory neurons ratio [73-77] and the fact glutamate clearance rate is modulated by the rate of firing [63, 91], it is not surprising that there is an overall elevated GCaMP and iGluSnFr activity of the 30 s pulse train (Fig. 8, 5-6). In contrast, the lasting inhibitory effects of the reinforced inhibitory network activity can be observed in the post-stimulus period under widefield GCaMP imaging. There is a prolonged inhibition of GCaMP activity after the stimulus train ends indicating a lingering inhibitory network effect, potentially further influenced by GABA spillover acting on $GABA_B$ receptors[77, 85]. Future studies should examine the influence of TP on GABA activity. Analysis of the GCaMP neuropil activity over the first two seconds and last two seconds of the 30 s pulse train indicates that the excitatory network is strongly driven over the first two seconds compared to the last two seconds. This change in neuropil activity over time suggests that the influence of inhibitory network activity is strengthened with uniform high frequency stimulation, even if excitatory neuronal elements can be directly and strongly driven without entrainment (Fig. 7C). Although we cannot conclusively say that these effects are due to inhibition, the results presented here highly support the idea that there is a major influence and motivates further investigation into its role.

### 5.4 Temporal Patterning on Onset neuronal activity during ICMS

In order to understand why the different temporal patterns resulted in different soma-neuropil correlations (Fig. 7D), it is important to examine the mechanism underlying Onset neuron activity (Fig. 4). We established earlier that with 100 Hz stimulation, excitatory neurons are unable to entrain to high frequency pulse trains. Instead, excitatory neurons with sufficient neuronal elements that pass through the small direct activation volume (yellow circle Fig. 9) are driven to depolarize within 10 ms of the end of the absolute refractory period. In turn, the excitatory network (composed of a majority of the cells in the cortex: 75~80%) is significantly strengthened over the first 2 s of the stimulus pulse train leading to a strong post-synaptic neuronal activation (Fig. 9 Left). During this onset period, the inhibitory network has not likely reached its full inhibitory strength, allowing for a broad post-synaptic onset activation pattern. However, as the 100 Hz uniform stimulation pulse train persists, the post-synaptic inhibitory inputs begin suppressing downstream neurons that were initially driven by the strong excitatory network activation at the beginning of the pulse train. This leads to some decrease in the excitatory neuropil activity and the inhibition of onset neurons resulting in a decreased soma-neuropil correlation (Fig. 7; Fig. 9 Right). On the other hand, this onset effect was minimal and comparable between 10 Hz-Burst and 10 Hz-Uniform. For 10 Hz-Burst there is strong inhibitory network activation during the first 100 ms of each stimulation burst (Fig. S1), however the 900ms break between bursts does not continue to drive the inhibitory network resulting in relatively strong direct and post-synaptic excitatory neural activation at 1 Hz (Fig 4). Conversely, for 10 Hz-Uniform, the greatest balance of excitatory and inhibitory neuronal activation may have led to the lowest steady-state somas (Fig. 4D) and lowest soma-neuropil correlation (Fig. 7D). This can again be explained by the idea that most neurons, whether excitatory or inhibitory, have high entrainment probability to 10 Hz stimulation, and because excitatory neurons outweigh inhibitory neurons in number and activation probability (myelination, branching)[92, 93], the excitatory drive overshadows the inhibitory drive (Fig. 9; Fig. S1).

For all stimulation patterns, there are significantly more steady state cells compared to onset cells (Fig. 4D). While there are no significant differences between the number of onset cells for each pattern, 10 Hz-Burst has the least number of onset neurons and has a minimal onset effect within the neuropil. For 10 Hz-Burst onset neurons, it remains to be determined if these are post-synaptic onset excitatory neurons that entrain at frequencies below 1 Hz or post-synaptic inhibitory neurons experiencing disinhibition. The latter is unlikely, as only 1% of the GCaMP+ cells are inhibitory [78]. However, it is still possible that we are observing the

downstream effects of inhibitory-excitatory loops. For example, in sensory cortex, it has been described that excitatory neurons can recruit vasointestinal peptide (VIP) inhibitory neurons[104]. In turn, these VIP neurons inhibit somatostatin (SOM)-expressing inhibitory neurons that disinhibit SOM post-synaptic pyramidal neurons. Thus, because this inhibitory drive at the onset of each stimulation burst in 10 Hz-Burst is not continuously driven during each 900ms inter-burst interval allowing for some disinhibition, a more stable activation pattern was observed, yet with overall elevated inhibition. Conversely, for 10 Hz-Uniform, the 10 Hz stimulation may lead to greater excitatory onset neuronal activity patterns. Although most neurons are able to entrain at 8 Hz stimulation [80], there are some neurons that can only entrain at lower frequencies. Additionally, inhibitory neurons provide more synapses onto target neurons, thus potentially providing a stronger effect on some excitatory neurons for each individual pulse [77]. While the present study cannot conclusively determine a potential sequence of activation of different inhibitory and excitatory cell types, future studies using dual labels to identify neuronal subtypes will further elucidate the mechanisms underlying onset neuronal activity to ICMS [105].

### 5.5 Neuronal preference to temporal patterning for neural prosthetics

Natural sensation involves a high dimensional neural activation with precise rate codes, therefore accurate control of the temporal code of neural activation is critical to increase the dynamic range of possible artificial sensations in neural prosthetics [17, 20, 106, 107]. Electrical stimulation of neurons depends on several factors including the geometry of axonal branching, the distance to the nearest node of Ranvier, the density of ion channels in proximal neuronal compartments, and the recovery cycle [87, 90, 92, 96, 108, 109]. Our glutamate sensor results indicate that direct orthodromic neural recruitment is strongest within 20μm of the electrode with rapid spatial drop off (Fig. 5-6). This means that the neuronal element composition immediately surrounding the electrode is extremely influential in determining which neural networks are recruited during stimulation to produce neural firing rates that would be elevated for one pattern but not another (Fig. 2-3). Specifically, the presence and subtype of interneurons within the immediate vicinity of the electrode could have a large impact on sculpting neural activity. In fact, interneurons were suggested to have a major role in the efficiency of bladder contraction induced by pudendal nerve stimulation with different temporal patterns [110]. In particular, out of all the temporal patterns with the same average frequency, the two patterns that interrupted interneuron firing resulted in the weakest contractions [110]. This could suggest that the different preference for the temporal patterns investigated here may be a result of differential activation of inhibitory neurons having unique roles in the inhibitory-excitatory balance[89].

Although neural firing rate codes are certainly important to elicit specific and diverse artificial perceptions, precise control over the network oscillations may offer another dimension to ICMS. Within the visual cortex, active sensing of the visual field can produce specific neural oscillations that correlate with the rate of saccadic eye movements (reviewed [111]), and measurements of neural oscillations were demonstrated to be correlated with the performance in a tactile task [112]. Here, we demonstrate 10 Hz-burst elicited strong inhibitory recruitment at distant locations from the electrode compared to 10 Hz-Uniform, which had the same number of pulses (Fig. 8). Additionally, both glutamate release and calcium activity contained a large 1Hz component in the power spectrum demonstrating that the temporal pattern of stimulation could drive specific oscillations with different weights of inhibition and excitation. Therefore, the ability to not only control the spike timing of different neurons, but also the network oscillations despite the variability excitatory and inhibitory neuronal neurons around the electrode will be critical to improve restoration of artificial sensation.

Due to the complexity of electrical stimulation, many studies investigate changing one or two parameters and measure the perception or broad neural activation around the electrode[4, 17, 35, 37, 113]. We have previously shown that stimulation waveform[37], amplitude[35], frequency[32], and here temporal pattern, can modulate the spatial and temporal activation of neurons which ultimately controls network activity. Varied combinations of these protocols may be necessary in order to design successful biomimetic stimulation protocols specific to the neural and glial composition around the electrode. Therefore, future work should investigate the response patterns of the diverse subtypes of inhibitory neurons to a multitude of stimulation parameters and their impact on the network balance in order to improve the ability to encode more complex sensations.

## 6. Conclusion

Using *in vivo* mesoscale and two-photon imaging of calcium activity within neuron soma and neuropil as well as glutamate activity, we demonstrate that temporal pattern of stimulation has a major impact on the differential recruitment of subsets of neurons, neuropil, excitatory neurotransmitter release ultimately driving different levels of excitation and inhibition. Subsets of neurons prefer specific temporal patterns of stimulation, which was highly correlated to the temporal activity of the neuropil. Neuropil, soma, and glutamate release were shown to have a significant entrainment to the carrier frequency of stimulation delivered every 1s for 100 ms. This further provides evidence that stimulation can be used to phase lock neuronal network activation at different frequencies. Finally, mesoscale imaging demonstrated that these subtle differences between the temporal patterns may arise from differential control over inhibitory and excitatory network oscillations during stimulation. Combining temporal patterning with exciting stimulation parameters may offer a new avenue to control spatiotemporal firing rates and network oscillation in the design of biomimetic stimulation protocols to restore impaired sensory processing. Together, we show that temporal patterning is a valuable tool for fundamental science research as well as prosthetic applications.

## 7. Acknowledgments

We would like to thank Prof. Alberto L. Vazquez for assistance and training for the viral injections. This work was supported by NIH R01NS094396, R01NS105691, and R21NS108098, NSF CAREER 1943906, and the ARCS Foundation, Inc., Pittsburgh Chapter, Gookin Family Foundation Award. The authors would also like to thank Prof. Warren Grill for constructive discussions.

References

[1] K.L. Clark, K.M. Armstrong, T. Moore, Probing neural circuitry and function with electrical microstimulation, Proceedings. Biological sciences 278(1709) (2011) 1121-30.
[2] D.L. Byrd, W.J. Marks, Jr., P.A. Starr, Deep brain stimulation for advanced Parkinson's disease, AORN journal 72(3) (2000) 387-90, 393-408; quiz 409-14, 416-8.
[3] H.S. Mayberg, A.M. Lozano, V. Voon, H.E. McNeely, D. Seminowicz, C. Hamani, J.M. Schwalb, S.H. Kennedy, Deep Brain Stimulation for Treatment-Resistant Depression, Neuron 45(5) (2005) 651-660.
[4] S.N. Flesher, J.L. Collinger, S.T. Foldes, J.M. Weiss, J.E. Downey, E.C. Tyler-Kabara, S.J. Bensmaia, A.B. Schwartz, M.L. Boninger, R.A. Gaunt, Intracortical microstimulation of human somatosensory cortex, Sci Transl Med 8(361) (2016) 361ra141.
[5] J.E. O'Doherty, M.A. Lebedev, Z. Li, M.A. Nicolelis, Virtual active touch using randomly patterned intracortical microstimulation, IEEE transactions on neural systems and rehabilitation engineering : a publication of the IEEE Engineering in Medicine and Biology Society 20(1) (2012) 85-93.
[6] G.A. Tabot, J.F. Dammann, J.A. Berg, F.V. Tenore, J.L. Boback, R.J. Vogelstein, S.J. Bensmaia, Restoring the sense of touch with a prosthetic hand through a brain interface, Proceedings of the National Academy of Sciences of the United States of America 110(45) (2013) 18279-84.
[7] B.S. Wilson, C.C. Finley, D.T. Lawson, R.D. Wolford, D.K. Eddington, W.M. Rabinowitz, Better speech recognition with cochlear implants, Nature 352(6332) (1991) 236-8.
[8] J.A. Berg, J.F. Dammann, 3rd, F.V. Tenore, G.A. Tabot, J.L. Boback, L.R. Manfredi, M.L. Peterson, K.D. Katyal, M.S. Johannes, A. Makhlin, R. Wilcox, R.K. Franklin, R.J. Vogelstein, N.G. Hatsopoulos, S.J. Bensmaia, Behavioral demonstration of a somatosensory neuroprosthesis, IEEE transactions on neural systems and rehabilitation engineering : a publication of the IEEE Engineering in Medicine and Biology Society 21(3) (2013) 500-7.
[9] R. Romo, A. Hernandez, A. Zainos, C.D. Brody, L. Lemus, Sensing without touching: psychophysical performance based on cortical microstimulation, Neuron 26(1) (2000) 273-8.
[10] R. Romo, A. Hernandez, A. Zainos, E. Salinas, Somatosensory discrimination based on cortical microstimulation, Nature 392(6674) (1998) 387-90.

[11] M. Armenta Salas, L. Bashford, S. Kellis, M. Jafari, H. Jo, D. Kramer, K. Shanfield, K. Pejsa, B. Lee, C.Y. Liu, R.A. Andersen, Proprioceptive and cutaneous sensations in humans elicited by intracortical microstimulation, eLife 7 (2018).
[12] N. Cicmil, K. Krug, Playing the electric light orchestra—how electrical stimulation of visual cortex elucidates the neural basis of perception, Philosophical Transactions of the Royal Society B: Biological Sciences 370(1677) (2015).
[13] E.M. Schmidt, M.J. Bak, F.T. Hambrecht, C.V. Kufta, D.K. O'Rourke, P. Vallabhanath, Feasibility of a visual prosthesis for the blind based on intracortical microstimulation of the visual cortex, Brain : a journal of neurology 119 ( Pt 2) (1996) 507-22.
[14] E.J. Tehovnik, W.M. Slocum, Microstimulation of macaque V1 disrupts target selection: effects of stimulation polarity, Experimental brain research 148(2) (2003) 233-7.
[15] E.J. Tehovnik, W.M. Slocum, P.H. Schiller, Saccadic eye movements evoked by microstimulation of striate cortex, The European journal of neuroscience 17(4) (2003) 870-8.
[16] S. Kim, T. Callier, G.A. Tabot, R.A. Gaunt, F.V. Tenore, S.J. Bensmaia, Behavioral assessment of sensitivity to intracortical microstimulation of primate somatosensory cortex, Proceedings of the National Academy of Sciences 112(49) (2015) 15202-15207.
[17] T. Callier, N.W. Brantly, A. Caravelli, S.J. Bensmaia, The frequency of cortical microstimulation shapes artificial touch, Proceedings of the National Academy of Sciences 117(2) (2020) 1191-1200.
[18] G.Y. Fridman, H.T. Blair, A.P. Blaisdell, J.W. Judy, Perceived intensity of somatosensory cortical electrical stimulation, Experimental brain research 203(3) (2010) 499-515.
[19] I. Birznieks, R.M. Vickery, Spike Timing Matters in Novel Neuronal Code Involved in Vibrotactile Frequency Perception, Current biology : CB 27(10) (2017) 1485-1490.e2.
[20] H.P. Saal, X. Wang, S.J. Bensmaia, Importance of spike timing in touch: an analogy with hearing?, Current opinion in neurobiology 40 (2016) 142-149.
[21] D.L. Kimmel, T. Moore, Temporal patterning of saccadic eye movement signals, Journal of Neuroscience 27(29) (2007) 7619-7630.
[22] W.M. Grill, Temporal Pattern of Electrical Stimulation is a New Dimension of Therapeutic Innovation, Current opinion in biomedical engineering 8 (2018) 1-6.
[23] C.W. Hess, D.E. Vaillancourt, M.S. Okun, The temporal pattern of stimulation may be important to the mechanism of deep brain stimulation, Exp Neurol 247 (2013) 296-302.
[24] A. Hernández, A. Zainos, R. Romo, Neuronal correlates of sensory discrimination in the somatosensory cortex, Proceedings of the National Academy of Sciences 97(11) (2000) 6191.
[25] S. Butovas, S.G. Hormuzdi, H. Monyer, C. Schwarz, Effects of electrically coupled inhibitory networks on local neuronal responses to intracortical microstimulation, J Neurophysiol 96(3) (2006) 1227-36.
[26] S. Butovas, C. Schwarz, Spatiotemporal effects of microstimulation in rat neocortex: a parametric study using multielectrode recordings, J Neurophysiol 90(5) (2003) 3024-39.
[27] J.A. Gomez, J.M. Perkins, G.M. Beaudoin, N.B. Cook, S.A. Quraishi, E.A. Szoeke, K. Thangamani, C.W. Tschumi, M.J. Wanat, A.M. Maroof, M.J. Beckstead, P.A. Rosenberg, C.A. Paladini, Ventral tegmental area astrocytes orchestrate avoidance and approach behavior, Nat Commun 10(1) (2019) 1455.
[28] J. Zhang, S. Zhang, C. Yu, X. Zheng, K. Xu, Intrinsic optical imaging study on cortical responses to electrical stimulation in ventral posterior medial nucleus of thalamus, Brain Res 1684 (2018) 40-49.
[29] S.N. Margalit, H. Slovin, Spatio-temporal characteristics of population responses evoked by microstimulation in the barrel cortex, Scientific reports 8(1) (2018) 13913.
[30] M. Osanai, S. Tanaka, Y. Takeno, S. Takimoto, T. Yagi, Spatiotemporal properties of the action potential propagation in the mouse visual cortical slice analyzed by calcium imaging, PLoS One 5(10) (2010) e13738.
[31] Y. Tanaka, T. Nomoto, T. Shiki, Y. Sakata, Y. Shimada, Y. Hayashida, T. Yagi, Focal activation of neuronal circuits induced by microstimulation in the visual cortex, J Neural Eng 16(3) (2019) 036007.

[32] N.J. Michelson, J.R. Eles, A.L. Vazquez, K.A. Ludwig, T.D.Y. Kozai, Calcium activation of cortical neurons by continuous electrical stimulation: Frequency dependence, temporal fidelity, and activation density, J Neurosci Res 97(5) (2019) 620-638.
[33] J.R. Eles, T.D.Y. Kozai, In vivo imaging of calcium and glutamate responses to intracortical microstimulation reveals distinct temporal responses of the neuropil and somatic compartments in layer II/III neurons. , Biomaterials (2020).
[34] N.J. Michelson, T.D.Y. Kozai, Isoflurane and Ketamine Differentially Influence Spontaneous and Evoked Laminar Electrophysiology in Mouse V1, J Neurophysiol (2018).
[35] J.R. Eles, T.D.Y. Kozai, In vivo imaging of calcium and glutamate responses to intracortical microstimulation reveals distinct temporal responses of the neuropil and somatic compartments in layer II/III neurons, Biomaterials 234 (2020) 119767.
[36] N.J. Michelson, J.R. Eles, A.L. Vazquez, K.A. Ludwig, T.D.Y. Kozai, Calcium activation of cortical neurons by continuous electrical stimulation: Frequency dependence, temporal fidelity, and activation density, J Neurosci Res (2018).
[37] K.C. Stieger, J.R. Eles, K.A. Ludwig, T.D.Y. Kozai, In vivo microstimulation with cathodic and anodic asymmetric waveforms modulates spatiotemporal calcium dynamics in cortical neuropil and pyramidal neurons of male mice, Journal of Neuroscience Research n/a(n/a).
[38] A. Sanzeni, B. Akitake, H.C. Goldbach, C.E. Leedy, N. Brunel, M.H. Histed, Inhibition stabilization is a widespread property of cortical networks, eLife 9 (2020) e54875.
[39] D.R. Merrill, M. Bikson, J.G. Jefferys, Electrical stimulation of excitable tissue: design of efficacious and safe protocols, J Neurosci Methods 141(2) (2005) 171-98.
[40] Q. Chen, J. Cichon, W. Wang, L. Qiu, S.-Jin R. Lee, Nolan R. Campbell, N. DeStefino, Michael J. Goard, Z. Fu, R. Yasuda, Loren L. Looger, Benjamin R. Arenkiel, W.-B. Gan, G. Feng, Imaging Neural Activity Using Thy1-GCaMP Transgenic Mice, Neuron 76(2) (2012) 297-308.
[41] J.S. Marvin, B.G. Borghuis, L. Tian, J. Cichon, M.T. Harnett, J. Akerboom, A. Gordus, S.L. Renninger, T.W. Chen, C.I. Bargmann, M.B. Orger, E.R. Schreiter, J.B. Demb, W.B. Gan, S.A. Hires, L.L. Looger, An optimized fluorescent probe for visualizing glutamate neurotransmission, Nature methods 10(2) (2013) 162-70.
[42] J.R. Eles, A.L. Vazquez, T.D.Y. Kozai, X.T. Cui, In vivo imaging of neuronal calcium during electrode implantation: Spatial and temporal mapping of damage and recovery, Biomaterials 174 (2018) 79-94.
[43] S. Eick, J. Wallys, B. Hofmann, A. Van Ooyen, U. Schnakenberg, S. Ingebrandt, A. Offenhäusser, Iridium oxide microelectrode arrays for in vitro stimulation of individual rat neurons from dissociated cultures, Frontiers in Neuroengineering 2(16) (2009).
[44] N.J. Michelson, J.R. Eles, A.L. Vazquez, K.A. Ludwig, T.D.Y. Kozai, Calcium activation of cortical neurons by continuous electrical stimulation: Frequency dependence, temporal fidelity, and activation density, Journal of Neuroscience Research 97(5) (2019) 620-638.
[45] T.D.Y. Kozai, A.S. Jaquins-Gerstl, A.L. Vazquez, A.C. Michael, X.T. Cui, Dexamethasone retrodialysis attenuates microglial response to implanted probes in vivo, Biomaterials 87 (2016) 157-169.
[46] J.R. Eles, A.L. Vazquez, T.D.Y. Kozai, X.T. Cui, Meningeal inflammatory response and fibrous tissue remodeling around intracortical implants: An in vivo two-photon imaging study, Biomaterials 195 (2019) 111-123.
[47] J.R. Eles, A.L. Vazquez, N.R. Snyder, C.F. Lagenaur, M.C. Murphy, T.D.Y. Kozai, X.T. Cui, Neuroadhesive L1 coating attenuates acute microglial attachment to neural electrodes as revealed by live two-photon microscopy, Biomaterials 113 (2017) 279-292.
[48] T.D.Y. Kozai, J.R. Eles, A.L. Vazquez, X.T. Cui, Two-photon imaging of chronically implanted neural electrodes: Sealing methods and new insights, Journal of Neuroscience Methods 258 (2016) 46-55.
[49] S.M. Wellman, T.D.Y. Kozai, In vivo spatiotemporal dynamics of NG2 glia activity caused by neural electrode implantation, Biomaterials 164 (2018) 121-133.

[50] N.J. Michelson, A.L. Vazquez, J.R. Eles, J.W. Salatino, E.K. Purcell, J.J. Williams, X.T. Cui, T.D.Y. Kozai, Multi-scale, multi-modal analysis uncovers complex relationship at the brain tissue-implant neural interface: New Emphasis on the Biological Interface, J Neural Eng 15(033001) (2018).
[51] T.D.Y. Kozai, A.L. Vazquez, C.L. Weaver, S.-G. Kim, X.T. Cui, In vivo two-photon microscopy reveals immediate microglial reaction to implantation of microelectrode through extension of processes, J Neural Eng 9(6) (2012) 066001-066001.
[52] T.D.Y. Kozai, X. Li, L.M. Bodily, E.M. Caparosa, G.A. Zenonos, D.L. Carlisle, R.M. Friedlander, X.T. Cui, Effects of caspase-1 knockout on chronic neural recording quality and longevity: Insight into cellular and molecular mechanisms of the reactive tissue response., Biomaterials 35(36) (2014) 9620-9634.
[53] T.D.Y. Kozai, T.C. Marzullo, F. Hooi, N.B. Langhals, A.K. Majewska, E.B. Brown, D.R. Kipke, Reduction of neurovascular damage resulting from microelectrode insertion into the cerebral cortex using in vivo two-photon mapping., Journal of neural engineering 7 (2010) 046011.
[54] S.N. Flesher, J.L. Collinger, S.T. Foldes, J.M. Weiss, J.E. Downey, E.C. Tyler-Kabara, S.J. Bensmaia, A.B. Schwartz, M.L. Boninger, R.A. Gaunt, Intracortical microstimulation of human somatosensory cortex, Science translational medicine 8(361) (2016) 361ra141-361ra141.
[55] M.H. Histed, V. Bonin, R.C. Reid, Direct activation of sparse, distributed populations of cortical neurons by electrical microstimulation, Neuron 63(4) (2009) 508-22.
[56] E.J. Tehovnik, W.M. Slocum, Two-photon imaging and the activation of cortical neurons, Neuroscience 245 (2013) 12-25.
[57] J. Akerboom, T.-W. Chen, T.J. Wardill, L. Tian, J.S. Marvin, S. Mutlu, N.C. Calderón, F. Esposti, B.G. Borghuis, X.R. Sun, A. Gordus, M.B. Orger, R. Portugues, F. Engert, J.J. Macklin, A. Filosa, A. Aggarwal, R. Kerr, R. Takagi, S. Kracun, E. Shigetomi, B.S. Khakh, H. Baier, L. Lagnado, S.S.H. Wang, C.I. Bargmann, B.E. Kimmel, V. Jayaraman, K. Svoboda, D.S. Kim, E.R. Schreiter, L.L. Looger, Optimization of a GCaMP calcium indicator for neural activity imaging, The Journal of neuroscience : the official journal of the Society for Neuroscience 32(40) (2012) 13819-13840.
[58] S. Zhou, Y. Yu, Synaptic E-I Balance Underlies Efficient Neural Coding, Frontiers in neuroscience 12(46) (2018).
[59] J.-S. Jouhanneau, J. Kremkow, J.F.A. Poulet, Single synaptic inputs drive high-precision action potentials in parvalbumin expressing GABA-ergic cortical neurons in vivo, Nature Communications 9(1) (2018) 1540.
[60] C.C. Petersen, S. Crochet, Synaptic computation and sensory processing in neocortical layer 2/3, Neuron 78(1) (2013) 28-48.
[61] C.-Y.T. Li, M.-M. Poo, Y. Dan, Burst spiking of a single cortical neuron modifies global brain state, Science (New York, N.Y.) 324(5927) (2009) 643-646.
[62] H. Dana, T.W. Chen, A. Hu, B.C. Shields, C. Guo, L.L. Looger, D.S. Kim, K. Svoboda, Thy1-GCaMP6 transgenic mice for neuronal population imaging in vivo, PLoS One 9(9) (2014) e108697.
[63] M. Armbruster, E. Hanson, C.G. Dulla, Glutamate Clearance Is Locally Modulated by Presynaptic Neuronal Activity in the Cerebral Cortex, J Neurosci 36(40) (2016) 10404-10415.
[64] A. McGirr, J. LeDue, A.W. Chan, Y. Xie, T.H. Murphy, Cortical functional hyperconnectivity in a mouse model of depression and selective network effects of ketamine, Brain : a journal of neurology 140(8) (2017) 2210-2225.
[65] N.J. Michelson, T.D.Y. Kozai, Isoflurane and Ketamine Differentially Influence Spontaneous and Evoked Laminar Electrophysiology in Mouse V1, J Neurophysiol (2018).
[66] A.C. Kwan, Y. Dan, Dissection of cortical microcircuits by single-neuron stimulation in vivo, Current biology : CB 22(16) (2012) 1459-1467.
[67] H.K. Chan, D.-P. Yang, C. Zhou, T. Nowotny, Burst Firing Enhances Neural Output Correlation, Front Comput Neurosci 10 (2016) 42-42.
[68] J.N.D. Kerr, W. Denk, Imaging in vivo: watching the brain in action, Nature Reviews Neuroscience 9 (2008) 195.

[69] J.N.D. Kerr, D. Greenberg, F. Helmchen, Imaging input and output of neocortical networks in vivo, Proceedings of the National Academy of Sciences of the United States of America 102(39) (2005) 14063.
[70] S. Lee, J.F. Meyer, J. Park, S.M. Smirnakis, Visually Driven Neuropil Activity and Information Encoding in Mouse Primary Visual Cortex, Frontiers in Neural Circuits 11(50) (2017).
[71] D.T. Brocker, B.D. Swan, R.Q. So, D.A. Turner, R.E. Gross, W.M. Grill, Optimized temporal pattern of brain stimulation designed by computational evolution, Sci Transl Med 9(371) (2017).
[72] J. Cabral, E. Hugues, O. Sporns, G. Deco, Role of local network oscillations in resting-state functional connectivity, Neuroimage 57(1) (2011) 130-139.
[73] J. Sloper, An electron microscopic study of the neurons of the primate motor and somatic sensory cortices, Journal of neurocytology 2(4) (1973) 351-359.
[74] S.H. Hendry, H. Schwark, E. Jones, J. Yan, Numbers and proportions of GABA-immunoreactive neurons in different areas of monkey cerebral cortex, Journal of Neuroscience 7(5) (1987) 1503-1519.
[75] P. Gabbott, P. Somogyi, Quantitative distribution of GABA-immunoreactive neurons in the visual cortex (area 17) of the cat, Experimental brain research 61(2) (1986) 323-331.
[76] C.A. Anastassiou, R. Perin, G. Buzsaki, H. Markram, C. Koch, Cell type- and activity-dependent extracellular correlates of intracellular spiking, J Neurophysiol 114(1) (2015) 608-23.
[77] H. Markram, M. Toledo-Rodriguez, Y. Wang, A. Gupta, G. Silberberg, C. Wu, Interneurons of the neocortical inhibitory system, Nat Rev Neurosci 5(10) (2004) 793-807.
[78] H. Makino, C. Ren, H. Liu, A.N. Kim, N. Kondapaneni, X. Liu, D. Kuzum, T. Komiyama, Transformation of Cortex-wide Emergent Properties during Motor Learning, Neuron 94(4) (2017) 880-890.e8.
[79] S. Lodato, C. Rouaux, K.B. Quast, C. Jantrachotechatchawan, M. Studer, T.K. Hensch, P. Arlotta, Excitatory projection neuron subtypes control the distribution of local inhibitory interneurons in the cerebral cortex, Neuron 69(4) (2011) 763-779.
[80] S.H. Bitzenhofer, J. Ahlbeck, A. Wolff, J.S. Wiegert, C.E. Gee, T.G. Oertner, I.L. Hanganu-Opatz, Layer-specific optogenetic activation of pyramidal neurons causes beta-gamma entrainment of neonatal networks, Nat Commun 8 (2017) 14563.
[81] H. Ozeki, I.M. Finn, E.S. Schaffer, K.D. Miller, D. Ferster, Inhibitory stabilization of the cortical network underlies visual surround suppression, Neuron 62(4) (2009) 578-92.
[82] S.-i. Amari, Dynamics of pattern formation in lateral-inhibition type neural fields, Biological cybernetics 27(2) (1977) 77-87.
[83] M.A. Harvey, H.P. Saal, J.F. Dammann, 3rd, S.J. Bensmaia, Multiplexing stimulus information through rate and temporal codes in primate somatosensory cortex, PLoS Biol 11(5) (2013) e1001558.
[84] P. Tiesinga, T.J. Sejnowski, Cortical enlightenment: are attentional gamma oscillations driven by ING or PING?, Neuron 63(6) (2009) 727-32.
[85] G. Tamas, A. Lorincz, A. Simon, J. Szabadics, Identified sources and targets of slow inhibition in the neocortex, Science 299(5614) (2003) 1902-5.
[86] A.M. Thomson, A. Destexhe, Dual intracellular recordings and computational models of slow inhibitory postsynaptic potentials in rat neocortical and hippocampal slices, Neuroscience 92(4) (1999) 1193-215.
[87] G. Yi, W.M. Grill, Frequency-dependent antidromic activation in thalamocortical relay neurons: effects of synaptic inputs, J Neural Eng 15(5) (2018) 056001.
[88] Y. Tanaka, T. Nomoto, T. Shiki, Y. Sakata, Y. Shimada, Y. Hayashida, T. Yagi, Focal activation of neuronal circuits induced by microstimulation in the visual cortex, Journal of Neural Engineering 16(3) (2019) 036007.
[89] R. Tremblay, S. Lee, B. Rudy, GABAergic Interneurons in the Neocortex: From Cellular Properties to Circuits, Neuron 91(2) (2016) 260-92.
[90] C.C. McIntyre, W.M. Grill, D.L. Sherman, N.V. Thakor, Cellular effects of deep brain stimulation: model-based analysis of activation and inhibition, J Neurophysiol 91(4) (2004) 1457-69.
[91] M.P. Parsons, M.P. Vanni, C.L. Woodard, R. Kang, T.H. Murphy, L.A. Raymond, Real-time imaging of glutamate clearance reveals normal striatal uptake in Huntington disease mouse models, Nature Communications 7(1) (2016) 11251.

[92] A.S. Aberra, A.V. Peterchev, W.M. Grill, Biophysically realistic neuron models for simulation of cortical stimulation, J Neural Eng 15(6) (2018) 066023.
[93] C. Overstreet, J. Klein, S.H. Tillery, Computational modeling of direct neuronal recruitment during intracortical microstimulation in somatosensory cortex, J Neural Eng 10(6) (2013) 066016.
[94] E.J. Tehovnik, W.M. Slocum, Two-photon imaging and the activation of cortical neurons, Neuroscience (2013).
[95] T.D.Y. Kozai, N.A. Alba, H. Zhang, N.A. Kotov, R.A. Gaunt, X.T. Cui, Nanostructured Coatings for Improved Charge Delivery to Neurons, in: M. De Vittorio, L. Martiradonna, J. Assad (Eds.), Nanotechnology and Neuroscience: Nano-electronic, Photonic and Mechanical Neuronal Interfacing, Springer New York, New York, NY, 2014, pp. 71-134.
[96] M. Radivojevic, D. Jackel, M. Altermatt, J. Muller, V. Viswam, A. Hierlemann, D.J. Bakkum, Electrical Identification and Selective Microstimulation of Neuronal Compartments Based on Features of Extracellular Action Potentials, Scientific reports 6 (2016) 31332.
[97] J.C. Octeau, M.R. Gangwani, S.L. Allam, D. Tran, S. Huang, T.M. Hoang-Trong, P. Golshani, T.H. Rumbell, J.R. Kozloski, B.S. Khakh, Transient, Consequential Increases in Extracellular Potassium Ions Accompany Channelrhodopsin2 Excitation, Cell Reports 27(8) (2019) 2249-2261.e7.
[98] Z. Guo, Z. Feng, Y. Wang, X. Wei, Simulation Study of Intermittent Axonal Block and Desynchronization Effect Induced by High-Frequency Stimulation of Electrical Pulses, Frontiers in neuroscience 12(858) (2018).
[99] Y. Wang, A. Gupta, M. Toledo-Rodriguez, C.Z. Wu, H. Markram, Anatomical, physiological, molecular and circuit properties of nest basket cells in the developing somatosensory cortex, Cereb Cortex 12(4) (2002) 395-410.
[100] D.R. Serwanski, C.P. Miralles, S.B. Christie, A.K. Mehta, X. Li, A.L. De Blas, Synaptic and nonsynaptic localization of GABAA receptors containing the alpha5 subunit in the rat brain, The Journal of comparative neurology 499(3) (2006) 458-70.
[101] L.E. Lorenzo, M. Russier, A. Barbe, J.M. Fritschy, H. Bras, Differential organization of gamma-aminobutyric acid type A and glycine receptors in the somatic and dendritic compartments of rat abducens motoneurons, The Journal of comparative neurology 504(2) (2007) 112-26.
[102] T.W. Chen, T.J. Wardill, Y. Sun, S.R. Pulver, S.L. Renninger, A. Baohan, E.R. Schreiter, R.A. Kerr, M.B. Orger, V. Jayaraman, L.L. Looger, K. Svoboda, D.S. Kim, Ultrasensitive fluorescent proteins for imaging neuronal activity, Nature 499(7458) (2013) 295-300.
[103] J.P. Wikswo Jr, S.-F. Lin, R.A. Abbas, Virtual electrodes in cardiac tissue: a common mechanism for anodal and cathodal stimulation, Biophysical journal 69(6) (1995) 2195-2210.
[104] S. Lee, I. Kruglikov, Z.J. Huang, G. Fishell, B. Rudy, A disinhibitory circuit mediates motor integration in the somatosensory cortex, Nat Neurosci 16(11) (2013) 1662-70.
[105] M.B. Krawchuk, C.F. Ruff, X. Yang, S.E. Ross, A.L. Vazquez, Optogenetic assessment of VIP, PV, SOM and NOS inhibitory neuron activity and cerebral blood flow regulation in mouse somato-sensory cortex, Journal of Cerebral Blood Flow & Metabolism 0(0) (2019) 0271678X19870105.
[106] B.P. Delhaye, H.P. Saal, S.J. Bensmaia, Key considerations in designing a somatosensory neuroprosthesis, Journal of physiology, Paris 110(4 Pt A) (2016) 402-408.
[107] J.D. Lieber, S.J. Bensmaia, High-dimensional representation of texture in somatosensory cortex of primates, Proceedings of the National Academy of Sciences of the United States of America 116(8) (2019) 3268-3277.
[108] C.C. McIntyre, W.M. Grill, Extracellular stimulation of central neurons: influence of stimulus waveform and frequency on neuronal output, J Neurophysiol 88(4) (2002) 1592-604.
[109] J.B. Ranck, Jr., Which elements are excited in electrical stimulation of mammalian central nervous system: a review, Brain Res 98(3) (1975) 417-40.
[110] M.J. McGee, W.M. Grill, Temporal pattern of stimulation modulates reflex bladder activation by pudendal nerve stimulation, Neurourology and urodynamics 35(8) (2016) 882-887.

[111] M. Leszczynski, C.E. Schroeder, The Role of Neuronal Oscillations in Visual Active Sensing, Frontiers in Integrative Neuroscience 13(32) (2019).
[112] B.M. Adhikari, K. Sathian, C.M. Epstein, B. Lamichhane, M. Dhamala, Oscillatory activity in neocortical networks during tactile discrimination near the limit of spatial acuity, NeuroImage 91 (2014) 300-10.
[113] S. Kim, T. Callier, G.A. Tabot, R.A. Gaunt, F.V. Tenore, S.J. Bensmaia, Behavioral assessment of sensitivity to intracortical microstimulation of primate somatosensory cortex, Proceedings of the National Academy of Sciences of the United States of America 112(49) (2015) 15202-7.

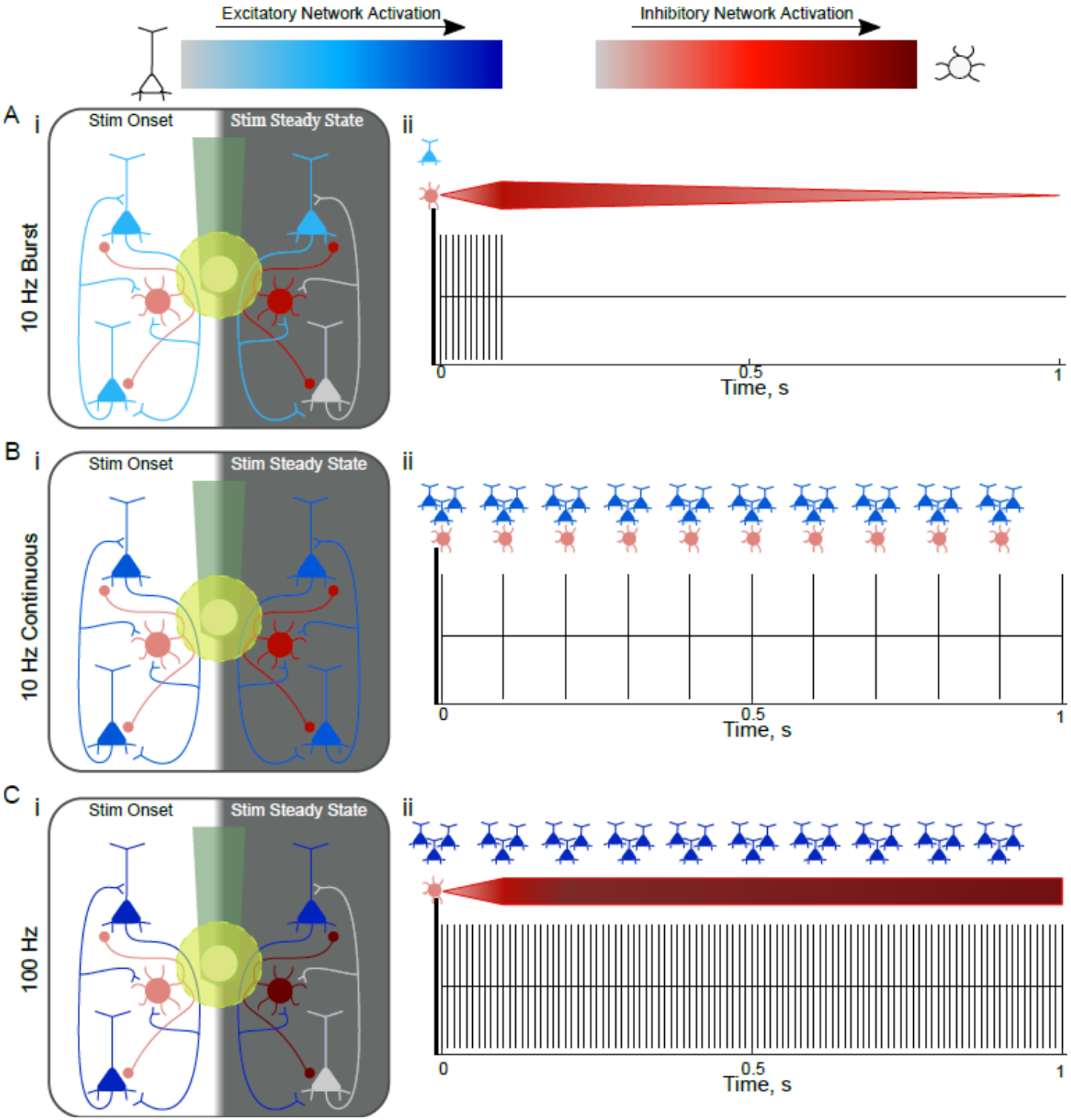


**Supplementary Figure 1: Temporal pattern of stimulation differentially drives excitatory and inhibitory network activation.** Representative diagram of possible activation patterns of directly activated or indirectly activated neurons (Ai-Ci) and their corresponding levels of network activation during 1s of the 30s stimulation

(Aii-Cii).During the onset period of all TPs (A: 10 Hz-Burst, B: 10 Hz-Uniform, C: 100 Hz), inhibitory network activation is low, with 10Hz-Burst having the lowest excitatory neuronal activation due to the pyramidal neurons absolute refractory period extending through the majority of the burst duration (~90ms). During the first 100 ms of 10 Hz-Burst (Aii) and 100 Hz (Cii), the inhibitory network oscillations strengthen leading to inactivation of neurons activated orthodromically (trans-synaptic activation; Right side of Ai, Ci). During this time, excitatory neurons cannot activate a second time, and the inhibitory network activation decreases for 10 Hz-Burst (Aii) or continues to increase for 100 Hz (Cii). Inhibitory network activation therefore outweighs that of the excitatory network in 10 Hz-Burst stimulation (A). For 100 Hz stimulation, however, because excitatory neurons outnumber inhibitory neurons and as soon as excitatory neuron's absolute refractory period ends, there is a stimulating pulse within 10 ms that depolarizes these neurons. The higher distribution of excitatory neurons in the cortex outweighs the inhibitory neurons leading to greater excitation near the electrode (C). In contrast, both excitatory and inhibitory network can entrain to 10 Hz stimulation, therefore this TP results in neural activation leads to a more balanced activation of excitation and inhibition (B).

Supplementary video captions.

Supplementary Video 1: Two-photon imaging during 10 Hz-Burst stimulation in *Thy1*-GCaMP6s mice over 30s activates cortical neurons with strong 1 Hz power and limited spatial fall off. Images captured at 30 frames per second (FPS), averaged to 5 FPS and played at 5X speed.

Supplementary Video 2: Two-photon imaging during 10 Hz-Uniform stimulation *Thy1*-GCaMP6s mice results in stable spatiotemporal recruitment of cortical neurons. Images captured at 30 FPS, averaged to 5 FPS and played at 5X speed.

Supplementary Video 3: Two-photon imaging during 100 Hz stimulation *Thy1*-GCaMP6s mice results in transient activation of distal neurons, with stable activation of neurons proximal to the electrode. Images captured at 30 FPS, averaged to 5 FPS and played at 5X speed.

Supplementary Video 4: Two-photon imaging during 10Hz-Burst stimulation in mice expressing the fluorescent glutamate sensor, iGluSnFR, under the hsyn promotor demonstrates limited glutamate release during 30s stimulation trains. Images captured at 30 FPS, averaged to 5 FPS and played at 5X speed.

Supplementary Video 5: Two-photon imaging during 10Hz-Unifrm stimulation in mice expressing the fluorescent glutamate sensor, iGluSnFR, under the hsyn promotor demonstrates minor glutamate release within 20 μm during 30s stimulation trains. Two-photon Images captured at 30 FPS, averaged to 5 FPS and played at 5X speed.

Supplementary Video 6: Two-photon imaging during 100Hz stimulation in mice expressing the fluorescent glutamate sensor, iGluSnFR, under the hsyn promotor demonstrates significant glutamate release within 20 μm during 30s stimulation trains. Images captured at 30 FPS, averaged to 5 FPS and played at 5X speed.

Supplementary Video 7: Widefield epifluorescence imaging during 10Hz-Burst stimulation in *Thy1*-GCaMP6s mice demonstrates substantial inhibitory network drive at distal locations. Images captured at 20 FPS, averaged down to 5 FPS played at 5X speed.

Supplementary Video 8: Widefield epifluorescence imaging during 10Hz-Uniform stimulation in *Thy1*-GCaMP6s mice demonstrates spatiotemporally stable and substantial excitatory network drive. Images captured at 20 FPS, averaged down to 5 FPS played at 5X speed.

Supplementary Video 9: Widefield epifluorescence imaging during 100Hz-Uniform stimulation in *Thy1*-GCaMP6s mice demonstrates transient excitatory followed by inhibitory network drive at distal locations. Images captured at 20 FPS, averaged down to 5 FPS played at 5X speed.